01 Jan 1985

UNSTEADY-STATE SPHERICAL FLOW WITH STORAGE AND SKIN.

Jeffrey A. Joseph

Leonard Koederitz

Missouri University of Science and Technology, koe@mst.edu

Unsteady-State Spherical Flow With Storage and Skin

Jeffrey A. Joseph,* SPE, U. of Missouri-Rolla
Leonard F. Koederitz, SPE, U. of Missouri-Rolla

Abstract

This paper presents short-time interpretation methods for radial-spherical (or radial-hemispherical) flow in homogeneous and isotropic reservoirs inclusive of wellbore storage, wellbore phase redistribution, and damage skin effects. New dimensionless groups are introduced to facilitate the classic transformation from radial flow in the sphere to linear flow in the rod. Analytical expressions, type curves (in log-log and semilog format), and tabulated solutions are presented, both in terms of pressure and rate, for all flow problems considered. A new empirical equation to estimate the duration of wellbore and near-wellbore effects under spherical flow is also proposed.

Introduction

The majority of the reported research on unsteady-state flow theory applicable to well testing usually assumes a cylindrical (typically a radial-cylindrical) flow profile because this condition is valid for many test situations. Certain well tests, however, are better modeled by assuming a spherical flow symmetry (e.g., wireline formation testing, vertical interference testing, and perhaps even some tests conducted in wellbores that do not fully penetrate the productive horizon or are selectively completed). Plugged perforations or blockage of a large part of an openhole interval may also promote spherical flow. Numerous solutions are available in the literature for almost every conceivable cylindrical flow problem; unfortunately, the companion spherical problem has not received as much attention, and comparatively few papers have been published on this topic.[1-9]

The most common inner boundary condition in well test analysis is that of a constant production rate. But with the advent of downhole tools capable of the simultaneous measurement of pressures and flow rates, this idealized inner boundary condition has been refined and more sophisticated models have been proposed.[9-14] Therefore, similar methods must be developed for spherical flow analysis, especially for short-time interpretations. This general problem has recently been addressed elsewhere.[9]

Theory

The fundamental linear partial differential equation (PDE)[15] describing fluid flow in an infinite medium characterized by a radial-spherical symmetry is

$$\frac{1}{r^2}\frac{\partial}{\partial r}\left(r^2\frac{\partial p}{\partial r}\right)=\frac{\phi\mu c}{k}\frac{\partial p}{\partial t}. \quad \ldots\ldots\ldots\ldots\ldots\ldots (1)$$

The assumptions incorporated into this diffusion equation are similar to those imposed on the radial-cylindrical diffusivity equation and are discussed at length in Ref. 9. In solving Eq. 1, the classic approach is illustrated by Carslaw and Jaeger[16] (later used by Chatas[1] and Brigham *et al.*[5]). According to Carslaw and Jaeger, mapping $b=pr$ will always reduce the problem of radial flow in the sphere (Eq. 1) to an equivalent problem of linear flow in the rod for which general solutions are usually known. (For example, see Ref. 17 for particular solutions in petroleum applications.)

Note that in this study, we assumed that the medium is spherically isotropic; hence k in Eq. 1 is the constant spherical permeability. This assumption, however, does not preclude analysis in systems possessing simple anisotropy (i.e., uniform but unequal horizontal and vertical permeability components). In this case, k as used in this paper should be replaced by $\bar{k}$, an equivalent or average (but constant) spherical permeability. Chatas[1] presented a suitable expression (his Eq. 10) obtained from a volume integral.

It is desirable to transform Eq. 1 to a nondimensional form, thereby rendering its applicability universal. The following new, dimensionless groups accomplish this and have the added feature that solutions are obtained directly in terms of the dimensionless pressure drop, p_D, not the usual b (or b_D) groups.[1,5]

$$p_D=\frac{4\pi k r_{sw}(p_i-p_{r,t})}{q\mu}. \quad \ldots\ldots\ldots\ldots\ldots\ldots (2)$$

$$t_D=\frac{k r_{sw}^2 t}{\phi\mu c r^4};\ r\geqq r_{sw}. \quad \ldots\ldots\ldots\ldots\ldots\ldots (3)$$

$$r_D=1-\frac{r_{sw}}{r};\ r\geqq r_{sw}. \quad \ldots\ldots\ldots\ldots\ldots\ldots (4)$$

The quantity r_{sw} is an equivalent or pseudospherical wellbore radius used to represent the actual cylindrical sink (or source) of radius r_w. (See Refs. 2, 4 through 6, and 18 for a complete discussion of the fictitious

*Now with Flopetrol-Johnston, Melun, France

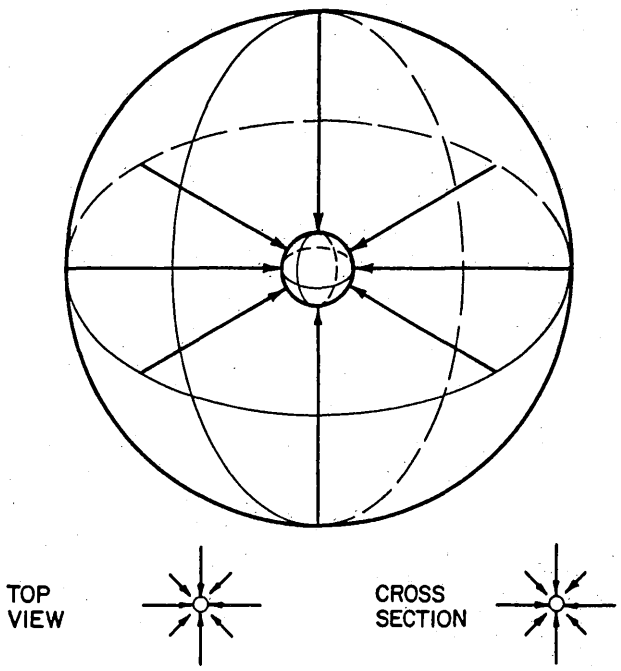

Fig. 1—Radial flow toward spherical sink wellbore.

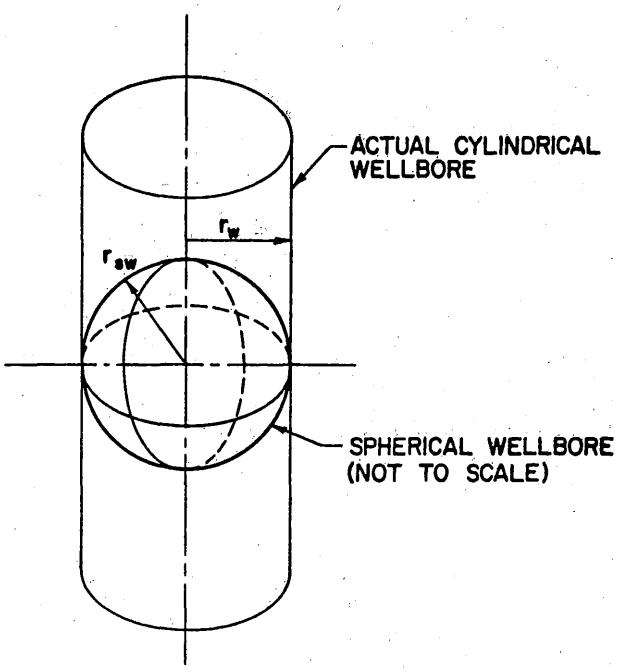

Fig. 2—Cylindrical and spherical wellbores.

spherical sink r_{sw}.) The physical system of interest is illustrated in Figs. 1 and 2. Fig. 1 depicts perfect radial flow in the sphere and shows that the region of accumulation (singularity) is itself a sphere of finite radius, r_{sw}. This singularity in the spherical model corresponds to a wellbore in the prototype, as shown in Fig. 2. (Note that the spherical wellbore in Fig. 2 is not to scale. A cylindrical wellbore radius of 5 in. [12.7 cm] may be represented by a pseudospherical wellbore radius of 3 ft [0.9 m]). We have obtained entirely satisfactory results using an equation for r_{sw} originally suggested by Moran and Finklea[2] and later used by Culham,[4] namely $r_{sw}=0.5b/\ln(b/r_w)$, where b is the length of the open or perforated interval. Note that the identities in Eqs. 2 through 4 are not defined in conventional fashion. For example, the transformation in Eq. 3 consolidates both independent variables t and r into a single expression for the dimensionless time, t_D. Variables of this type have been called similarity variables by several authors.[9] Substitution of Eqs. 2 through 4 into Eq. 1 yields[9,19]

$$\frac{\partial^2 p_D}{\partial r_D{}^2}=\frac{\partial p_D}{\partial t_D}. \quad \ldots\ldots\ldots\ldots\ldots\ldots\ldots\ldots\ldots\ldots (5)$$

Eq. 5 immediately is recognized as the diffusion equation in a medium characterized by a linear flow symmetry; we shall use Eq. 5 and the one-to-one[19] Transformations 2 through 4 to analyze the flow problem posed by Eq. 1. Hence, radial flow in the infinite sphere will be modeled by an equivalent problem of linear flow in the finite rod.

To produce particular solutions to Eq. 5, an initial boundary value problem (IBVP) must be posed and the initial and the general inner and outer boundary conditions must be specified. We now examine the values that the space variable r_D may assume. The inner boundary in r is obtained when $r=r_{sw}$ (i.e., the wellbore). From Eq. 4 we see that $r=r_{sw}$ corresponds to $r_D=0$. The original spherical system is unbounded in r; as r grows, r_D also grows, but in the limit as $r\to\infty$, r_D approaches unity. Particular solutions of Eq. 5 are developed in the following sections.

Constant Surface Rate With Skin and Storage

A very popular inner boundary condition in pressure-transient analysis is the stipulation of production at a constant surface rate from a wellbore of finite volume. Here we also will assume that a damage skin effect, s ($s\geqq 0$), exists at the sandface. The formation pressure drop is denoted by p_D, and the wellbore pressure drop is p_{wD}. The skin factor s represents a steady-state flow resistance at the sandface (i.e., zero storage capacity); this flow impediment establishes the relationship between p_{wD} and p_D. Let s be defined as

$$s=\frac{4\pi k r_{sw}\Delta p_s}{q_{sf}\mu}, \quad \ldots\ldots\ldots\ldots\ldots\ldots\ldots\ldots\ldots\ldots (6)$$

where Δp_s is the pressure drop across the infinitesimal skin zone (atm). Wellbore storage phenomena (i.e., the afterflow or unloading problem) will be described by C_D, the dimensionless coefficient of wellbore storage, defined as

$$C_D=\frac{C}{4\pi\phi c r_{sw}^3}, \quad \ldots\ldots\ldots\ldots\ldots\ldots\ldots\ldots\ldots\ldots (7)$$

where C represents the volume of wellbore fluid unloaded or stored. In the present formulation, C and hence C_D are considered constant.

The initial condition is taken as a constant pressure, p_i, for all values of $r \geqq r_{sw}$. Using Eqs. 2 and 4, we obtain

$$p_D(r_D, t_D=0)=0;\ 0 \leqq r_D \leqq 1. \quad \ldots\ldots\ldots\ldots\ldots\ldots (8)$$

We have considered the original spherical system infinite in radial extent because interest is focused on times short enough when pressure or rate disturbances at the inner boundary are not sensed at the outer boundary (or vice versa). This causes transience within the solution. Hence, the pressure at the outer boundary will be maintained at its initial value p_i for all time; thus

$$\lim_{r_D \to 1}[p_D(r_D, t_D)]=0;\ t_D>0. \quad \ldots\ldots\ldots\ldots\ldots\ldots (9)$$

The inner boundary condition was stated earlier. To obtain a solution in terms of the wellbore pressure, p_{wD}, one could either rewrite the original PDE (Eq. 1) in terms of p_{wD} or incorporate some known relationship between p_{wD} and p_D as an auxiliary condition. The latter approach is adopted here.

$$p_{wD}(t_D)=p_D(r_D=0, t_D)-s\left(\frac{\partial p_D}{\partial r_D}\right)_{r_D=0}. \quad \ldots\ldots (10)$$

Eq. 10 results from the definition of the skin effect (Eq. 6) and from a pressure drop at the sandface proportional to the dimensionless sandface flow rate. From Eq. 10 we note that the dimensionless sandface flow rate can be written in terms of the space derivative of p_D evaluated at the inner boundary:

$$\frac{q_{sf}}{q}=\left(\frac{\partial p_D}{\partial r_D}\right)_{r_D=0}. \quad \ldots\ldots\ldots\ldots\ldots\ldots\ldots (11)$$

A mass balance of the fluid in the wellbore reveals that the dimensionless sandface flow rate plus the dimensionless rate of wellbore unloading equals the constant surface rate (unity). Therefore, we conclude that

$$\frac{q_a}{q}=C_D\frac{dp_{wD}}{dt_D} \quad \ldots\ldots\ldots\ldots\ldots\ldots\ldots (12)$$

and that the combination of Eqs. 11 and 12 and the wellbore balance yields the inner boundary condition

$$C_D\frac{dp_{wD}}{dt_D}-\left(\frac{\partial p_D}{\partial r_D}\right)_{r_D=0}=1. \quad \ldots\ldots\ldots\ldots (13)$$

Thus far, we have established an initial-boundary-value problem in PDE's consisting of the PDE (Eq. 5), an initial condition (Eq. 8), an outer boundary condition (Eq. 9), and finally the inner boundary condition (Eq. 13). This boundary condition frequently is called a boundary condition of the second kind[20] or a Neumann condition.[21] The auxiliary condition (Eq. 10) will be used to obtain a solution in terms of the well pressure p_{wD}. This solution will describe the flow of a single-phase, slightly compressible fluid in a medium characterized by radial-spherical geometry, inclusive of wellbore storage and skin effects. To our knowledge, no such solutions have appeared in the literature.

The IBVP described earlier is amenable to solution by an operational technique, namely the Laplace transformation. Let

$$L[p_D(r_D, t_D)]=\int_0^\infty e^{-zt_D}\, p_D(r_D, t_D)dt_D$$

$$=\bar{p}_D(r_D, z), \quad \ldots\ldots\ldots\ldots\ldots (14)$$

where z is the Laplace variable of time, $z>0$. For our study, denoting the inverse Laplace transformation in functional form will suffice.

$$L^{-1}[\bar{p}_D(r_D, z)]=p_D(r_D, t_D). \quad \ldots\ldots\ldots\ldots (15)$$

Solutions to the IBVP in the Laplace domain are derived in Appendix A and are presented below:

$$\bar{p}_{wD}(z)=\frac{A+s\sqrt{z}B}{z^{3/2}\left[\sqrt{z}C_D\left(A+s\sqrt{z}B\right)+B\right]} \quad \ldots\ldots\ldots (16)$$

and

$$\bar{p}_D(r_D \geqq 0^+, z)=\frac{e^{-r_D\sqrt{z}}-e^{(r_D-2)\sqrt{z}}}{z^{3/2}\left[\sqrt{z}C_D\left(A+s\sqrt{z}B\right)+B\right]}, \quad \ldots\ldots\ldots\ldots\ldots\ldots (17)$$

where e denotes the exponential function, $A=1-e^{-2\sqrt{z}}$, and $B=1+e^{-2\sqrt{z}}$. Eq. 16 is the fundamental solution of interest in this paper, namely the well-pressure response in spherical systems influenced by storage and skin. Eq. 17 is the solution for the formation pressure drop. Both Eqs. 16 and 17 are valid for all time, for $s \geqq 0$, and for $C_D \geqq 0$.

Real-time (i.e., physical-space) solutions to Eq. 16 or 17 must be obtained by application of the inverse Laplace transformation (Eq. 15) because a closed-form inversion (perhaps with tables) does not appear possible. This may be achieved analytically with the Mellin inversion theorem.[16] For illustrative purposes, suppose $\bar{v}(z)$ is the Laplace transformation of $v(t)$; then

$$v(t)=\frac{1}{2\pi i}\lim_{\delta \to \infty}\int_{\gamma-i\delta}^{\gamma+i\delta} e^{zt}\,\bar{v}(z)dz;\ t>0, \quad \ldots\ldots\ldots (18)$$

where γ is so large that all the singularities of $\bar{v}(z)$ lie to the left of the line $(\gamma-i\infty, \gamma+i\infty)$. Here, $\bar{v}$ is considered to be a function of a complex variable, z, and $i=\sqrt{-1}$.

Eq. 18 is no longer very common in the petroleum literature, largely because of the numerical inversion

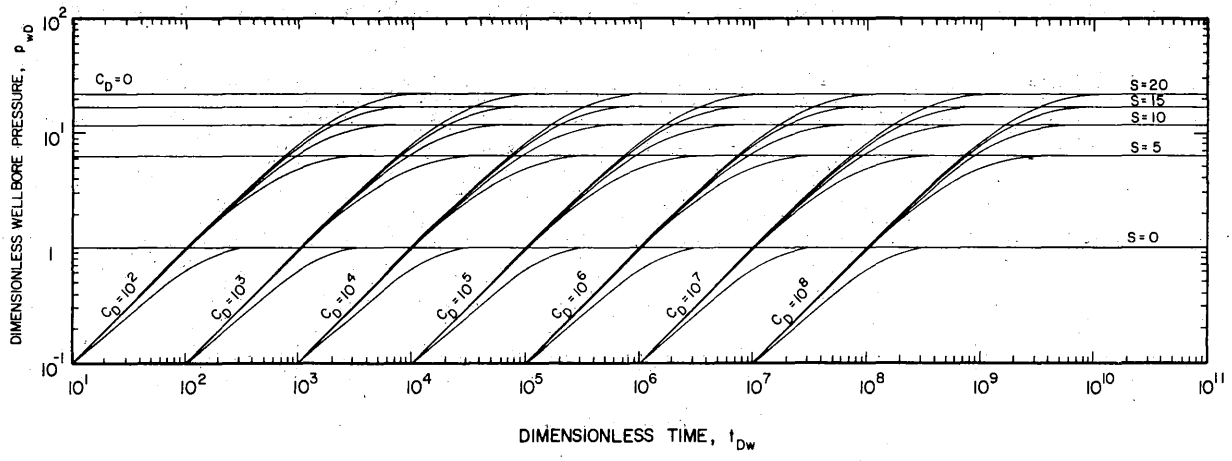

Fig. 3—Dimensionless wellbore pressure drop for a single well in an infinite spherical medium (spherical sink solution).

scheme of Stehfest.[22,23] This method is treated in detail elsewhere[9] and is not considered here. Here we only will report the value used for the inversion parameter N. All numerical calculations were performed on an Amdahl 470-V-7 machine with the IBM FORTRAN G1 compiler operating in Double Precision arithmetic.

Short- and Long-Time Approximations

It frequently is possible to approximate particular solutions by investigating the asymptotic behavior of the transform as the transformation variable (z) becomes large or small (short or long times). Details of this analysis are available in Appendix B; the results are presented here. For early time,

$$p_{wD}(t_D)=\frac{t_D}{C_D};\ s\geqq 0;\ C_D>0, \quad \ldots\ldots\ldots\ldots (19)$$

and for long time,

$$p_{wD}(t_D)=\sqrt{\frac{t_D}{\pi}}(1-e^{-1/t_D})+\operatorname{erfc}\left(\frac{1}{\sqrt{t_D}}\right)+s. \quad \ldots\ldots\ldots\ldots\ldots\ldots (20)$$

Eq. 16 is considered the general solution valid for all time, and the above approximation forms were produced from this expression. In Eqs. 19 and 20, t_D should be interpreted as t_{Dw}, where t_{Dw} is available from Eq. 3 as

$$t_{Dw}=\frac{kt}{\phi\mu c r_{sw}^2}. \quad \ldots\ldots\ldots\ldots\ldots\ldots (21)$$

Eq. 19 is the well-known formulation for depletion of the wellbore, which results in the familiar unit-slope portion on the log-log plot at early times (a log-log type curve is presented later). This equation is independent of flow symmetry. Short-time data exhibiting this behavior may be analyzed (as with the Ramey method[24]) to determine the coefficient of wellbore storage, C—i.e., the unit storage factor—for a spherical sink (source) wellbore.

It is shown in Appendix B that Eq. 20 reduces to the classic spherical source solutions. For short time,

$$p_{wD}(t_D)=2\sqrt{\frac{t_D}{\pi}}+s, \quad \ldots\ldots\ldots\ldots\ldots (22)$$

and for long time,

$$p_{wD}(t_D)=1-\frac{1}{\sqrt{\pi t_D}}+s. \quad \ldots\ldots\ldots\ldots\ldots (23)$$

So far, we have presented early- and long-time approximation forms of the general transformed solution (Eq. 16) for the problem of radial-spherical flow with wellbore storage and skin. One of these approximations (Eq. 20) was shown to reduce to the classic solutions (Eqs. 22 and 23) as special cases. For completeness, we also present below a rigorous equation applicable when $C_D=0$, which is usually a long-time phenomenon.[25,26]

$$p_{wD}(t_D)=4\sqrt{t_D}\left[\frac{1}{2\sqrt{\pi}}+\sum_{n+1}^{\infty}(-1)^n \times \operatorname{ierfc}\left(\frac{n}{\sqrt{t_D}}\right)\right]+s. \quad \ldots\ldots\ldots\ldots\ldots (24)$$

Eq. 20 is preferable to Eq. 24 because it is more tractable in applied and practical work.

Storage and Skin Type Curves

When short-time pressure-transient data are analyzed, one usually must resort to the popular technique of type-curve matching for problem resolution. Such methods are adequately described elsewhere.[24] Brigham *et al.*[5]

TABLE 1—p_{wD} (s, C_D, t_D) vs. t_{Dw} FOR SINGLE WELL IN INFINITE SPHERICAL MEDIUM (SPHERICAL SINK SOLUTION), p_{wD} vs. t_{Dw} FOR $s=0$ AT VARIOUS C_D

t_{Dw}	10^2	10^3	10^4	10^5	10^6	10^7	10^8
10^{-3}	0.000010	0.000001	0.000000	0.000000	0.000000	0.000000	0.000000
10^{-2}	0.000100	0.000010	0.000001	0.000000	0.000000	0.000000	0.000000
10^{-1}	0.000998	0.000100	0.000010	0.000001	0.000000	0.000000	0.000000
10^{0}	0.009921	0.000999	0.000100	0.000010	0.000001	0.000000	0.000000
10^{1}	0.094857	0.009948	0.001000	0.000100	0.000010	0.000001	0.000000
10^{2}	0.631618	0.095126	0.009951	0.001000	0.000100	0.000010	0.000001
10^{3}	1	0.632719	0.095153	0.009951	0.001000	0.000100	0.000010
10^{4}	1	1	0.632830	0.095156	0.009951	0.001000	0.000100
10^{5}	1	1	1	0.632841	0.095156	0.009951	0.001000
10^{6}	1	1	1	1	0.632842	0.095156	0.009951
10^{7}	1	1	1	1	1	0.632842	0.095156
10^{8}	1	1	1	1	1	1	0.632842
10^{9}	1	1	1	1	1	1	1

presented log-log type curves for spherical flow with wellbore storage effects but for the case $s=0$. To the best of our knowledge, type curves have not been developed yet for the general problem of spherical flow with storage and skin effects. We have selected the simplest plotting parameters, p_{wD} and t_{Dw}, and present log-log plots of these dimensionless groups as functions of s and C_D in Fig. 3. These type curves are for fully developed radial flow toward a finite, spherical sink wellbore within an infinite, homogeneous, isotropic medium. Fig. 3 was generated by numerical inversion of Eq. 16 with the Stehfest scheme[22,23]; the accuracy parameter N was set to 8 for all t_{Dw}.

It is well known[1,5] that the upper limit of the well-pressure response in an undamaged spherical medium is unity at infinite time; this is indeed verified upon inspection of Fig. 3. This figure also illustrates that the upper limit of the well-pressure response in a spherical medium with a damage skin effect, s, is equal to the steady-state (i.e., long-time) value at $s=0$ plus the magnitude s of the skin factor, for all values of C_D. In fact, this formal observation is also available directly from Eq. 20 or 23 and in Appendix B. This fascinating steady-state behavior at the wellbore—i.e., $p_{wD}=1+s$—while the formation is still being subjected to transient change is a feature unique to spherical flow. Portions of the data used to generate Fig. 3 are also presented in tabular form as Tables 1 and 2. (Additional tables are available in Ref. 9.) With appropriately selected values in a linear least-squares regression, the following approximate relationship when the wellbore pressure trace is no longer distorted by storage and skin effects was obtained.

$$t_D \geqq C_D(9.005+7.538\,s) \quad \ldots\ldots\ldots\ldots\ldots\ldots (25a)$$

or

$$t \geqq \frac{1{,}695C(9.005+7.538s)}{T}; \quad \ldots\ldots\ldots\ldots\ldots (25b)$$

where T is the spherical transmissivity group (kr_{sw}/μ) in field units. Regression results indicated that Eq. 25 should be accurate to within about 6% overall, and the computer program LSQ of Carlile and Gillett[27] helped model t_D/C_D as a first-degree polynomial in s. Eq. 25 provides a useful rule of thumb for test designing because the duration of wellbore and near-wellbore effects may be estimated. However, whether a test is conducted according to Eq. 25, the data should be curve matched with Fig. 3 in the conventional manner[24] to determine quantitatively the end of the wellbore-dominated period and to provide preliminary estimates of the spherical transmissivity group (kr_{sw}/μ) and the spherical porosity-compressibility product (ϕc_t). If sufficient test data are available, then Eq. 20 should be in-

TABLE 2—p_{wD} (s, C_D, t_D) vs. t_{Dw} FOR SINGLE WELL IN INFINITE SPHERICAL MEDIUM (SPHERICAL SINK SOLUTION), p_{wD} vs. t_{Dw} FOR $s=10$ AT VARIOUS C_D

t_{Dw}	10^2	10^3	10^4	10^5	10^6	10^7	10^8
10^{-3}	0.000010	0.000001	0.000000	0.000000	0.000000	0.000000	0.000000
10^{-2}	0.000100	0.000010	0.000001	0.000000	0.000000	0.000000	0.000000
10^{-1}	0.001000	0.000100	0.000010	0.000001	0.000000	0.000000	0.000000
10^{0}	0.009997	0.001000	0.000100	0.000010	0.000001	0.000000	0.000000
10^{1}	0.099558	0.009997	0.001000	0.000100	0.000010	0.000001	0.000000
10^{2}	0.955819	0.099560	0.009997	0.001000	0.000100	0.000010	0.000001
10^{3}	6.575987	0.955842	0.099560	0.009997	0.001000	0.000100	0.000010
10^{4}	11	6.576087	0.955844	0.099560	0.009997	0.001000	0.000100
10^{5}	11	11	6.576097	0.955844	0.099560	0.009997	0.001000
10^{6}	11	11	11	6.576098	0.955844	0.099560	0.009997
10^{7}	11	11	11	11	6.576098	0.955844	0.099560
10^{8}	11	11	11	11	11	6.576098	0.955844
10^{9}	11	11	11	11	11	11	6.576098
10^{10}	11	11	11	11	11	11	11

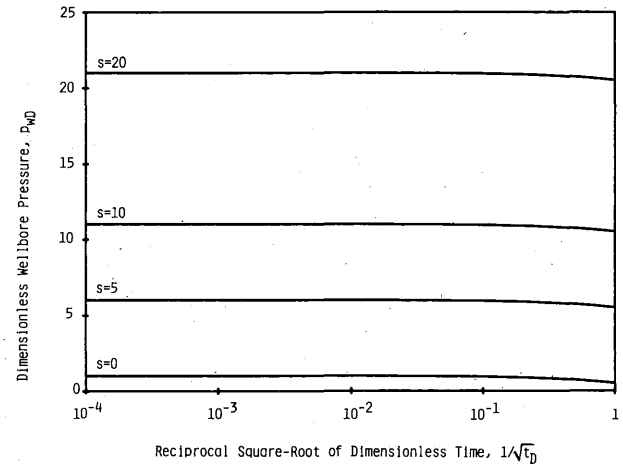

Fig. 4—Dimensionless wellbore pressure drop (long-time solution, Eq. 20) (spherical sink solution).

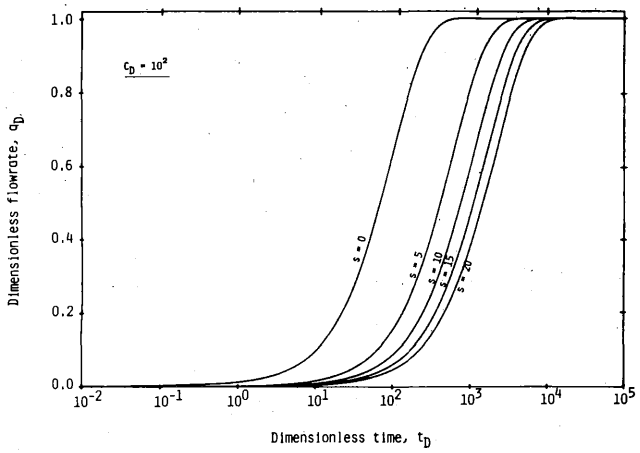

Fig. 5—Computed dimensionless sandface flow rate, q_D, vs. t_D for various skin effects, $C_D = 10^2$.

corporated into the analysis. Because this is a long-time approximation, it should not be applied to storage-influenced data. For example, Eq. 20 (presented graphically as Fig. 4) could be applied in accordance with the time criterion established by Eq. 25 or with the outcome of the preliminary type-curve analysis. Because the long-time approximation presented in this paper reduces to classic long-time solutions, all plots described in the literature[3,4,6,28] for static or flow tests remain applicable.

Dimensionless Sandface Flow Rate

The problem of well test interpretation using simultaneously measured pressures and sandface flow rates has been addressed recently in the literature.[9–14] The use of sandface flow rates, however, is not new. Van Everdingen[29] and Hurst[30] approximated q_{sf} by

$$\frac{q_{sf}}{q} = 1 - e^{-\beta t_D}. \quad \ldots\ldots\ldots\ldots\ldots\ldots\ldots\ldots\ldots\ldots (26)$$

Ramey and Agarwal[31] later presented tabular data and semilog plots of q_D vs. t_D and t_D/C_D for radial flow toward a cylindrical sink wellbore inclusive of a skin effect by numerical evaluation of a real inversion integral. Chatas[1] also identified a dimensionless rate function, e_D, and associated this with the dimensionless function

$$-\left(\frac{\partial p_D}{\partial r_D}\right)_{r_D=1}.$$

His results were presented in tabular format. However, plots similar to those of Ref. 31 have not appeared for the problem of spherical flow with storage. This gap is filled and extended to include spherical flow with storage and skin below.

Because the main effect of a storage coefficient is to cause the sandface flow rate, $q_{sf}(t)$, to change as the annulus unloads to supply a constant reference rate, q, we define a dimensionless sandface rate, q_D, as

$$q_D(t_D) = \frac{q_{sf}(t_D)}{q}, \quad \ldots\ldots\ldots\ldots\ldots\ldots\ldots\ldots\ldots\ldots (27)$$

assuming i annulus unloads to supply a constant reference rate, q, and iiC_D remains constant. By virtue of Eq. 11 through 13, two equivalent expressions for Eq.

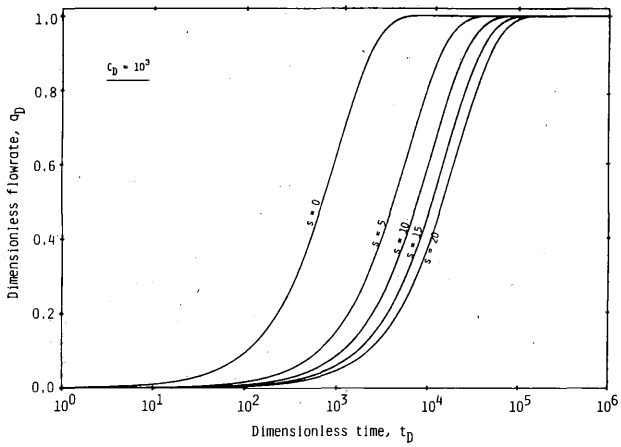

Fig. 6—Computed dimensionless sandface flow rate, q_D, vs. t_D for various skin effects, $C_D = 10^3$.

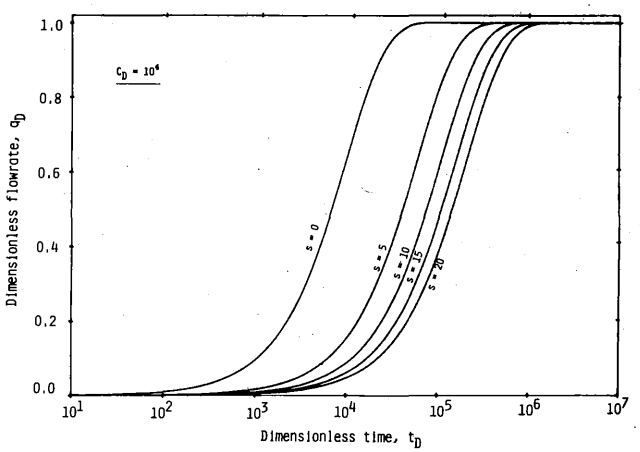

Fig. 7—Computed dimensionless sandface flow rate, q_D, vs. t_D for various skin effects, $C_D = 10^4$.

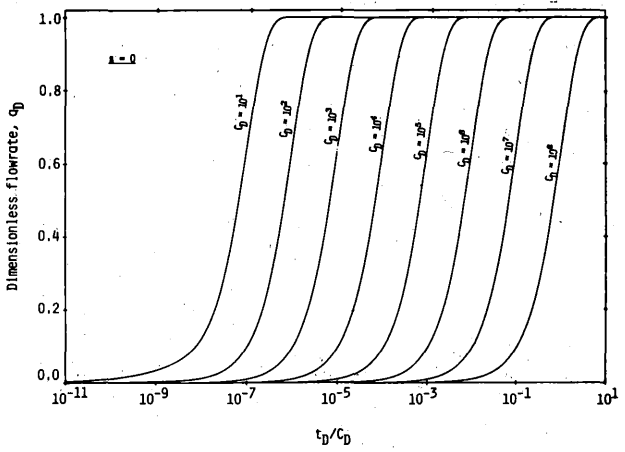

Fig. 8—Computed dimensionless sandface flow rate, q_D, vs. t_D/C_D for various wellbore storage coefficients $s=0$.

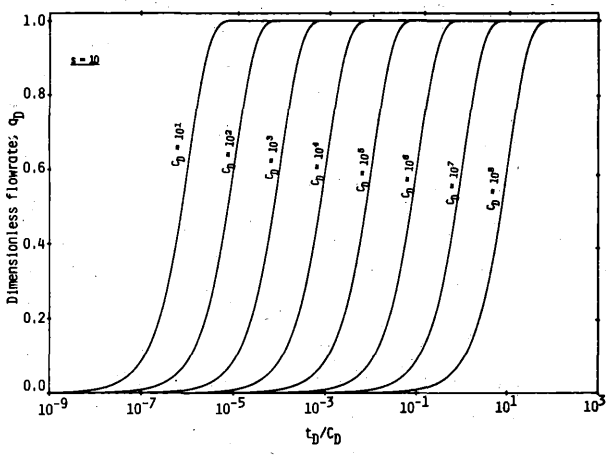

Fig. 9—Computed dimensionless sandface flow rate, q_D, vs. t_D/C_D for various wellbore storage coefficients, $s=10$.

27 are derived (in the Laplace domain) explicitly in Appendix C; Eq. C-6 is presented here as Eq. 28.

$$\bar{q}_D(z)=\frac{B}{z\left[\sqrt{z}C_D\left(A+s\sqrt{z}B\right)+B\right]}, \quad \ldots\ldots\ldots (28)$$

with A and B as defined for Eq. 16. Eq. 28 is the transformed solution for the sandface flow rate in a spherical system and is valid for $C_D \geqq 0$ and $s \geqq 0$. Note that $C_D=0$ implies that $q_D(t_D)=1$. Plots of q_D vs. log t_D and also log(t_D/C_D) were generated from Eq. 28 again with the Stehfest scheme,[22,23] with $N=8$. These plots are presented as Figs. 5 through 9 and in tabular format (q_D vs. t_D) in Tables 3 and 4. (Additional figures and tables are available from Ref. 9). As a check on the numerical inversion, Eqs. C-6 and C-7 were used, with less than 1% deviation in results. Inspection of these plots reveals that all the curves possess the same characteristic S-shaped nature as reported by Ramey and Agarwal[31] for perfect radial-cylindrical flow. Figs. 5 through 9 clearly illustrate the nature of the sandface flow rate as s and/or C_D are varied. The effect of an increase in s and/or C_D is to delay the time at which the downhole and surface rates become equal. As Ramey and Agarwal pointed out, these plots may also be used for type-curve matching.

Spherical Flow With Wellbore Phase Redistribution

The problems of pressure-buildup interpretation in the presence of wellbore-phase-redistribution effects has been studied previously.[32–35] Fair[32] recently presented type curves for the redistribution problem under cylindrical symmetry; however, he did not address the problem of sandface flow rates with phase redistributions within the wellbore. We now will extend Fair's corrected solutions for cylindrical and linear flow[9] and for spherical flow.

According to Fair, if phase-redistribution effects occur within a wellbore, wellbore storage must also occur. As envisioned, wellbore phase redistribution is also a form of wellbore storage. Hence, the additional storage effect can be incorporated into the transformed spherical IBVP presented earlier by means of the wellbore storage (inner boundary) condition. Because physical interpretations of the phase redistribution problem are available elsewhere,[9,32,35] we proceed directly with mathematical statements of the problem.

We begin by modifying the inner boundary condition (Eq. 13) as follows:

$$\frac{q_a}{q}+\frac{q_{sf}}{q}-\frac{q_\phi}{q}=1, \quad \ldots\ldots\ldots\ldots\ldots\ldots (29)$$

TABLE 3—q_D (s, C_D, t_D) vs. t_{Dw} DIMENSIONLESS SANDFACE FLOW RATES FOR VARIOUS WELLBORE STORAGE COEFFICIENTS AT $s=0$ (SPHERICAL SINK WELL)

t_{Dw}	10^1	10^2	10^3	10^4	10^5	10^6	10^7	10^8
10^{-3}	0.003558	0.000357	0.000036	0.000004	0.000000	0.000000	0.000000	0.000000
10^{-2}	0.011185	0.001127	0.000113	0.000011	0.000001	0.000000	0.000000	0.000000
10^{-1}	0.034717	0.003559	0.000357	0.000036	0.000004	0.000000	0.000000	0.000000
10^{0}	0.121885	0.013214	0.001332	0.000133	0.000013	0.000001	0.000000	0.000000
10^{1}	0.633098	0.097867	0.010278	0.001033	0.000103	0.000010	0.000001	0.000000
10^{2}	1	0.632843	0.095428	0.009984	0.001003	0.000100	0.000010	0.000001
10^{3}	1	1	0.632842	0.095183	0.009955	0.001000	0.000100	0.000010
10^{4}	1	1	1	0.632842	0.095159	0.009952	0.001000	0.000100
10^{5}	1	1	1	1	0.632842	0.095157	0.009952	0.001000
10^{6}	1	1	1	1	1	0.632842	0.095156	0.009951
10^{7}	1	1	1	1	1	1	0.632842	0.095156
10^{8}	1	1	1	1	1	1	1	0.632842
10^{9}	1	1	1	1	1	1	1	1

TABLE 4—q_D (s, C_D, t_D) vs. t_{Dw} DIMENSIONLESS SANDFACE FLOW RATES FOR VARIOUS WELLBORE STORAGE COEFFICIENTS AT $s=10$ (SPHERICAL SINK WELL)

t_{Dw}	10^1	10^2	10^3	10^4	10^5	10^6	10^7	10^8
10^{-3}	0.000010	0.000001	0.000000	0.000000	0.000000	0.000000	0.000000	0.000000
10^{-2}	0.000099	0.000010	0.000001	0.000000	0.000000	0.000000	0.000000	0.000000
10^{-1}	0.000976	0.000098	0.000010	0.000001	0.000000	0.000000	0.000000	0.000000
10^{0}	0.009304	0.000934	0.000093	0.000009	0.000001	0.000000	0.000000	0.000000
10^{1}	0.087125	0.009078	0.000912	0.000091	0.000009	0.000001	0.000000	0.000000
10^{2}	0.597837	0.086918	0.009054	0.000909	0.000091	0.000009	0.000001	0.000000
10^{3}	1	0.597828	0.086897	0.009051	0.000909	0.000091	0.000009	0.000001
10^{4}	1	1	0.597827	0.086895	0.009051	0.000909	0.000091	0.000009
10^{5}	1	1	1	0.597827	0.086895	0.009051	0.000909	0.000091
10^{6}	1	1	1	1	0.597827	0.086895	0.009051	0.000909
10^{7}	1	1	1	1	1	0.597827	0.086895	0.009051
10^{8}	1	1	1	1	1	1	0.597827	0.086895
10^{9}	1	1	1	1	1	1	1	0.597827
10^{10}	1	1	1	1	1	1	1	1

where q_ϕ is an additional flow rate associated with the phase redistribution pressure, p_ϕ. When $q_\phi=0$, Eqs. 13 and 29 become identical when Eqs. 11 and 12 are used as required. On the basis of a number of physical deductions, Fair concluded that this phase redistribution pressure (p_ϕ) must satisfy the following conditions:

$$\lim_{t\to 0}[p_\phi(t)]=0, \quad \ldots\ldots\ldots\ldots\ldots\ldots\ldots\ldots (30)$$

$$\lim_{t\to \infty}[p_\phi(t)]=C_\phi, \quad \ldots\ldots\ldots\ldots\ldots\ldots\ldots\ldots (31)$$

and

$$\lim_{t\to \infty}\left[\frac{dp_\phi(t)}{dt}\right]=0. \quad \ldots\ldots\ldots\ldots\ldots\ldots\ldots\ldots (32)$$

Here, C_ϕ is a constant.

As in Fair's study, our major assumption is that the following functional representation can be used to describe p_ϕ accurately:

$$p_\phi(t)=C_\phi(1-e^{-\gamma t}). \quad \ldots\ldots\ldots\ldots\ldots\ldots\ldots\ldots (33)$$

It is readily seen that Eq. 33 satisfies Eqs. 30 through 32. C_ϕ and γ are phase redistribution pressure and time parameters, respectively. Eq. 33 can be written in the dimensionless form of

$$p_{\phi D}(t_D)=C_{\phi D}(1-e^{-\gamma_D t_D}). \quad \ldots\ldots\ldots\ldots\ldots\ldots\ldots\ldots (34)$$

Here, $p_{\phi D}$ and $C_{\phi D}$ are obtained by the substitution of p_ϕ and C_ϕ, respectively, for Δp in Eq. 2, and γ_D is derived from Eq. 21.

$$\gamma_D=\frac{\gamma\phi\mu c r_{sw}^2}{k}. \quad \ldots\ldots\ldots\ldots\ldots\ldots\ldots\ldots (35)$$

With Eqs. 3, 11, 12, and 34, the modified wellbore storage-phase redistribution inner boundary condition (Eq. 29) becomes

$$C_D\frac{dp_{wD}}{dt_D}-\left(\frac{\partial p_D}{\partial r_D}\right)_{r_D=0}-C_D\frac{dp_{\phi D}}{dt_D}=1. \quad \ldots (36)$$

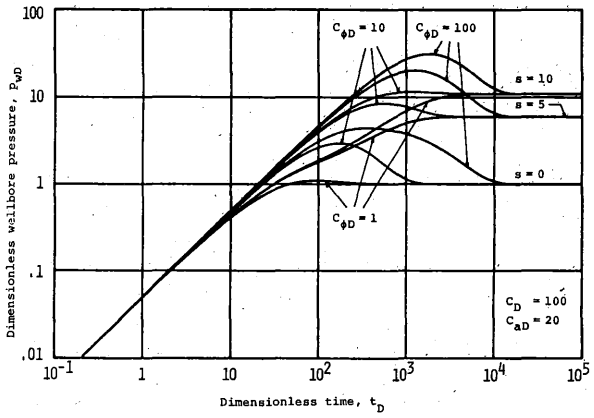

Fig. 10—p_{wD} vs. t_D with phase redistribution ($C_D=100$, $C_{aD}=20$) (spherical source solution).

Eq. 36 suggests that the redistribution flow rate $q_\phi=\gamma CC_\phi e^{-\gamma t}=CC_\phi f'(t)$ with $f(t)=1-e^{-\gamma t}$. The new IBVP inclusive of wellbore phase redistribution effects, therefore, is presented by Eqs. 5, 8 through 10, and 36. This problem is solved by Laplace transformation techniques in Appendix D, and Ref. 9 and is summarized below.

$$\bar{p}_{wD}(z)=\frac{(\gamma_D C_{aD}+zC_D)(A+s\sqrt{zB})}{(zC_{aD})(z+\gamma_D)\left[zC_D(A+s\sqrt{zB})+\sqrt{zB}\right]};\ C_{aD}\neq 0, \quad \ldots\ldots\ldots\ldots\ldots\ldots\ldots\ldots (37)$$

$$\bar{p}_D(r_D,z)=\frac{(\gamma_D C_{aD}+zC_D)\left[e^{-r_D\sqrt{z}}-e(r_D-2)\sqrt{z}\right]}{(zC_{aD})(z+\gamma_D)\left[zC_D(A+s\sqrt{zB})+\sqrt{zB}\right]};\ C_{aD}\neq 0, \quad \ldots\ldots\ldots\ldots\ldots\ldots\ldots\ldots (38)$$

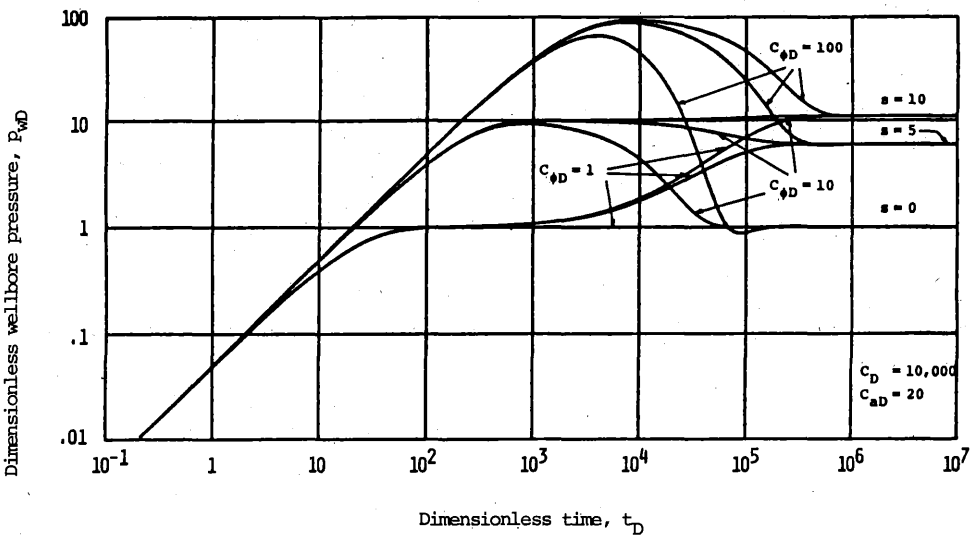

Fig. 11—p_{wD} vs. t_D with phase redistribution ($C_D = 10{,}000$, $C_{aD} = 20$) (spherical source solution).

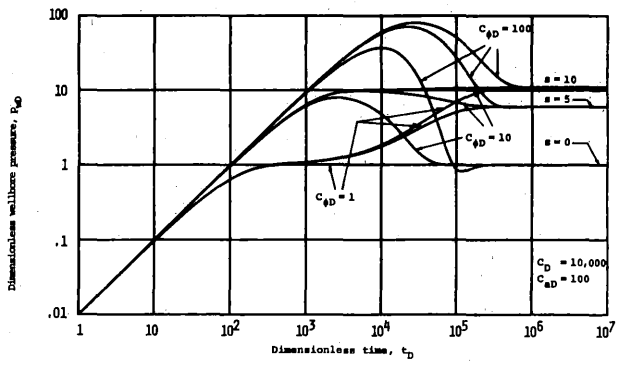

Fig. 12—p_{wD} vs. t_D with phase redistribution ($C_D = 10{,}000$, $C_{aD} = 100$) (spherical source solution).

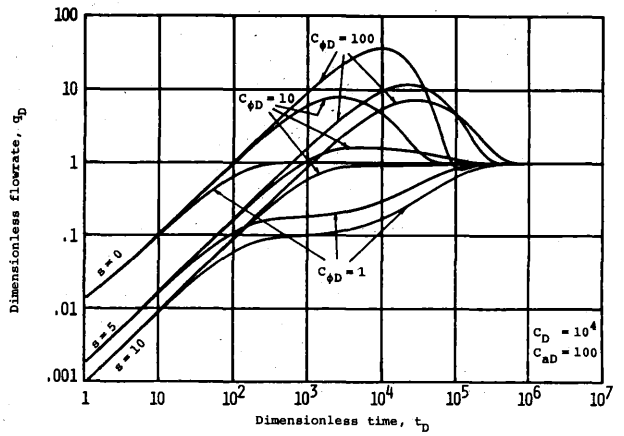

Fig. 13—q_D vs. t_D with phase redistribution ($C_D = 10{,}000$, $C_{aD} = 100$) (spherical source solution).

and

$$\bar{q}_D(z) = \frac{(\gamma_D C_{aD} + z C_D)B}{(zC_{aD})(z+\gamma_D)\left[\sqrt{z}C_D(A+s\sqrt{z}B)+B\right]};\ C_{aD} \neq 0. \quad \ldots\ldots\ldots\ldots\ldots\ldots\ldots\ldots\ldots\ldots (39)$$

A and B in Eqs. 37 through 39 are as defined earlier for Eq. 17. Eqs. 37 and 39 are the transformed solutions for the well pressure drop and sandface flow rate, respectively, in a spherical system inclusive of wellbore storage-phase redistribution and damage skin effects. Eq. 38 is the formation pressure drop in Laplace space. Further details of the derivations and additional forms of these solutions are contained in Ref. 9. C_{aD} is an apparent storage coefficient given by

$$C_{aD} = \frac{C_D}{1+\gamma_D C_D C_{\phi D}}. \quad \ldots\ldots\ldots\ldots\ldots\ldots\ldots\ldots\ldots\ldots (40)$$

We see from Eq. 40 that if $C_{\phi D} = 0$, the well exhibits a true wellbore storage effect controlled by C_D. Also, when $C_{aD} < C_D$, the storage effect usually is controlled by phase redistribution within the wellbore. (Refer to Ref. 9 or 32 for further details.) Eqs. 37 through 39 reduce to Eqs. 16, 17, and 28, respectively, by setting $C_{aD} = C_D$ and $\gamma_D = 0$.

Eqs. 37 and 39 are the solutions important to this study and were inverted by the Stehfest[22,23] algorithm with $N = 8$. Inversion results for Eq. 37 are presented graphically for selected values of s, C_D, C_{aD}, and $C_{\phi D}$ as a series of log-log type curves (Figs. 10, 11, and 12) and in tabular format in Tables 5 and 6. Inversion results for Eq. 39 also are presented as log-log type curves (Figs. 13 and 14) and in tabular format (Tables 7 and 8). Note that the abscissa of Fig. 14 is t_D/C_{aD}, which corresponds to a translation of the abscissa in Fig. 13. Additional inversion results and tables for several values of each parameter are available in Ref. 9.

TABLE 5—DIMENSIONLESS WELLBORE PRESSURES WITH PHASE REDISTRIBUTION EFFECTS (SPHERICAL SOURCE SOLUTION)

	$C_{aD}=20$, $C_D=100$		$C_{aD}=20$, $C_D=1{,}000$		$C_{aD}=20$, $C_D=10{,}000$	
	$s=0$	$s=10$	$s=0$	$s=10$	$s=0$	$s=10$
t_D	$C_{\phi D}=10$		$C_{\phi D}=10$		$C_{\phi D}=10$	
0.1	0.004988	0.005000	0.004998	0.005000	0.004999	0.005000
0.2	0.009965	0.009997	0.009993	0.009997	0.009996	0.009997
0.5	0.024849	0.024978	0.024960	0.024973	0.024971	0.024973
1	0.049524	0.049904	0.049847	0.049885	0.049879	0.049883
2	0.098385	0.099602	0.099403	0.099525	0.099504	0.099516
5	0.241125	0.247470	0.246345	0.246991	0.246867	0.246932
10	0.466642	0.489880	0.485585	0.487984	0.487510	0.487751
20	0.874391	0.959931	0.943479	0.952569	0.950751	0.951665
50	1.805476	2.259221	2.165192	2.217526	2.207099	2.212410
100	2.648381	4.098905	3.768170	3.956526	3.919613	3.939019
200	2.942951	6.811913	5.760100	6.386957	6.267837	6.334378
500	1.858361	10.465895	6.902719	9.327313	8.894482	9.177608
1,000	1.137152	11.527682	5.149665	10.181858	9.258115	9.958182
2,000	0.993844	11.327239	2.589199	10.332801	8.544737	10.044537
5,000	1.000124	11.020742	1.077270	10.484124	6.579279	10.060643
10,000	1.000478	10.997159	0.989468	10.673321	4.378993	10.103069
20,000	1.000090	10.999878	1.000790	10.867725	2.255846	10.181386
50,000	0.999998	11.000126	1.000572	10.990937	1.062651	10.377019
100,000	0.999997	11.000022	1.000068	11.000771	0.992130	10.605170
200,000	0.999999	11.000001	0.999993	10.999984	1.000690	10.839948
500,000	1.000000	11.000000	0.999996	10.999951	1.000447	10.989019

TABLE 6—DIMENSIONLESS WELLBORE PRESSURES WITH PHASE REDISTRIBUTION EFFECTS (SPHERICAL SOURCE SOLUTION)

	$C_{aD}=100$, $C_D=1{,}000$		$C_{aD}=100$, $C_D=10{,}000$		$C_{aD}=100$, $C_D=100{,}000$	
	$s=0$	$s=10$	$s=0$	$s=10$	$s=0$	$s=10$
t_D	$C_{\phi D}=100$		$C_{\phi D}=100$		$C_{\phi D}=100$	
10	0.099442	0.099929	0.099913	0.099962	0.099960	0.099965
20	0.197808	0.199685	0.199627	0.199816	0.199810	0.199829
50	0.486567	0.497922	0.497581	0.498735	0.498699	0.498815
100	0.947339	0.991556	0.990226	0.994793	0.994655	0.995113
200	1.796806	1.966067	1.960849	1.978932	1.978389	1.980209
500	3.851276	4.789563	4.757990	4.868463	4.865138	4.876365
1,000	6.039374	9.175610	9.055070	9.481064	9.468119	9.512166
2,000	7.774535	16.848027	16.407650	17.990863	17.941671	18.111225
5,000	7.230581	32.710934	30.566826	38.611168	38.344819	39.293392
10,000	5.023407	43.031396	37.216274	60.663830	59.803596	63.014407
20,000	2.640650	38.277485	27.519798	78.316290	75.972339	85.501779
50,000	1.115512	16.294378	4.926827	73.099884	67.006831	96.231818
100,000	0.990562	10.980655	0.865937	50.955538	41.527908	93.191376
200,000	1.000152	10.929697	0.955340	27.150192	16.017079	85.964135
500,000	1.000613	11.012290	1.011427	12.103135	1.743956	68.054495
1,000,000	1.000083	11.003013	1.002347	10.905690	0.905197	47.162181
2,000,000	0.999995	11.000232	1.000123	11.002221	1.009322	25.659311
5,000,000	0.999995	10.999942	0.999942	11.006012	1.005392	12.005823
10,000,000	0.999998	10.999975	0.999977	11.000802	1.000607	10.915012
20,000,000	1.000000	10.999992	0.999993	10.999949	0.999925	11.001948
50,000,000	1.000000	10.999999	0.999999	10.999955	0.999956	11.005414

The pressure type curves (Figs. 10 through 12) qualitatively resemble Fair's[32] type curves for cylindrical flow; i.e., the "hump" sometimes associated with wellbore phase segregations is also obtained under spherical formation flow. One would intuitively expect a profound impact of the segregation upon the wellbore pressure drop because pressure gradients are localized near the small-radius boundary (i.e., the wellbore) in a spherical system with a much greater concentration than in a radial-cylindrical system.[15] The infinite spherical reservoir, however, possesses a characteristic the unlimited cylindrical reservoirs do not possess: the well-pressure response is bounded at large times and is equal to the value of $(1+s)$ for all C_D and C_{aD}. The effect of the phase redistribution upon sandface flow rates is seen best by the comparison of Tables 3 and 4 with Tables 7 and 8 because the rate type curves with and without redistribution (Figs. 5 through 9, 13, and 14) contain different ordinates; the former are full logarithmic while the latter are semilogarithmic plots. Values of the dimensionless sandface rate q_D in excess of unity can be attributed to the phase redistribution phenomenon. These, however, all approach unity at long times. Although not as useful as the pressure type curves (Figs. 10 through 12), the rate type curves (Figs. 13 and 14) could be used in normal fashion for the interpretation of well test data

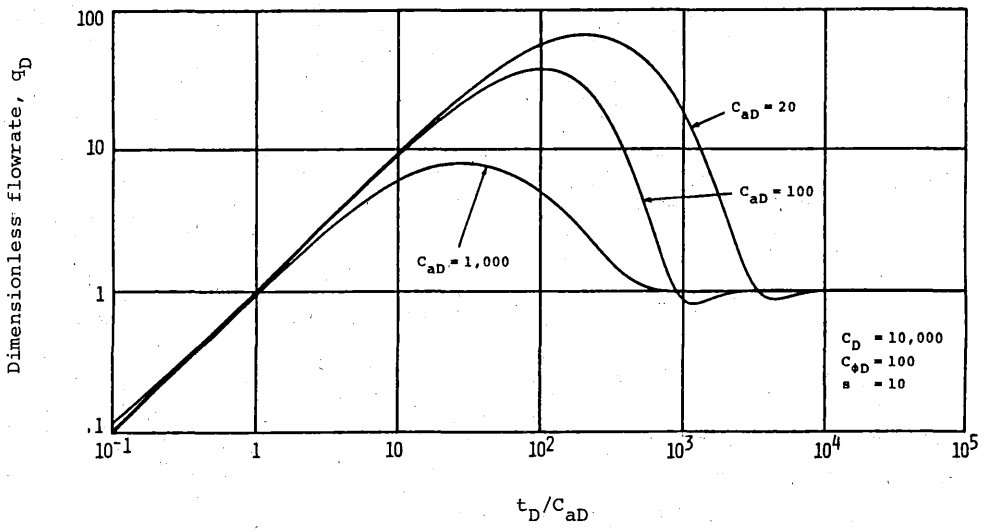

Fig. 14—q_D vs. t_D/C_{aD} with phase redistribution ($C_D = 10{,}000$, $C_{\varphi D} = 100$, $s = 10$) (spherical source solution).

distorted by wellbore storage (inclusive of phase redistributions) and skin effect. However, sandface flow rates must be recorded for such an analysis to be feasible.

Example

Table 9 presents the pressure-time data for a drawdown test simulated by a finite difference model.[19] Perfect radial-spherical flow has been assumed within the formation, which has a true spherical permeability of 88 md and spherical skin factor of 4.8. The value of r_{sw} shown in Table 9 was computed by the Moran and Finklea[2] approximation and later used by Culham.[4] Fig. 15 is the type-curve match for the test, which was performed with a gridded version of Fig. 3. As seen from Fig. 15, the early test data are dominated by wellbore storage. A match was obtained with the type curve for $s=5$ and $C_D=1{,}000$. The intersection of the type curve for $s=5$ and $C_D=0$ with the test data occurs at about $t=35.5$ hours (Fig. 15). The match points chosen are $(p_{wD})_M=0.67$, $(t_D)_M=8{,}128$, $(\Delta p)_M=100$ psi [6.89 MPa], and $(t)_M=10$ hours.

The following equations may be used to estimate the spherical permeability-radius product and the porosity-compressibility product from the pressure and time matches, respectively.

$$(kr_{sw})=70.627qB\mu\frac{(p_D)_M}{(\Delta p)_M} \quad \ldots\ldots\ldots\ldots\ldots\ldots (41)$$

TABLE 7—DIMENSIONLESS SANDFACE FLOW RATES WITH WELLBORE PHASE REDISTRIBUTION (SPHERICAL SOURCE SOLUTION)

	$C_{aD}=20$, $C_D=100$		$C_{aD}=20$, $C_D=1{,}000$		$C_{aD}=20$, $C_D=10{,}000$	
	$s=0$	$s=10$	$s=0$	$s=10$	$s=0$	$s=10$
t_D	$C_{\phi D}=10$		$C_{\phi D}=10$		$C_{\phi D}=10$	
0.1	0.017794	0.000488	0.017837	0.000488	0.017841	0.000488
0.2	0.025141	0.000967	0.025226	0.000967	0.025234	0.000967
0.5	0.041293	0.002373	0.041505	0.002372	0.041526	0.002372
1	0.065941	0.004664	0.066427	0.004663	0.066475	0.004662
2	0.114577	0.009191	0.115877	0.009184	0.116006	0.009183
5	0.256685	0.022632	0.262535	0.022588	0.263120	0.022583
10	0.481195	0.044667	0.501310	0.044494	0.503356	0.044472
20	0.887087	0.087394	0.958307	0.086722	0.965811	0.086640
50	1.813689	0.205496	2.177589	0.201701	2.220024	0.201236
100	2.651816	0.372719	3.777251	0.359769	3.929614	0.358176
200	2.942460	0.619325	5.764632	0.580684	6.273782	0.575903
500	1.857322	0.951461	6.902191	0.847950	8.895622	0.834340
1,000	1.136956	1.047972	5.148406	0.925625	9.257954	0.905290
2,000	0.993853	1.029748	2.588655	0.939346	8.544472	0.913140
5,000	1.000125	1.001886	1.077246	0.953102	6.579095	0.914604
10,000	1.000477	0.999742	0.989472	0.970302	4.378881	0.918461
20,000	1.000090	0.999989	1.000790	0.987975	2.255804	0.925581
50,000	0.999998	1.000011	1.000572	0.999176	1.062649	0.943365
100,000	0.999997	1.000002	1.000067	1.000070	0.992130	0.964106
200,000	0.999999	1.000000	0.999993	0.999999	1.000690	0.985450
500,000	1.000000	1.000000	0.999996	0.999996	1.000447	0.999002

TABLE 8—DIMENSIONLESS SANDFACE FLOW RATES WITH WELLBORE PHASE REDISTRIBUTION (SPHERICAL SOURCE SOLUTION)

	$C_{aD}=100$, $C_D=1{,}000$		$C_{aD}=100$, $C_D=10{,}000$		$C_{aD}=100$, $C_D=100{,}000$	
	$s=0$	$s=10$	$s=0$	$s=10$	$s=0$	$s=10$
t_D	$C_{\phi D}=100$		$C_{\phi D}=100$		$C_{\phi D}=100$	
10	0.102738	0.009112	0.103239	0.009115	0.103290	0.009115
20	0.201070	0.018181	0.202947	0.018193	0.203136	0.018194
50	0.489724	0.045293	0.500881	0.045367	0.502014	0.045374
100	0.950329	0.090169	0.993493	0.090463	0.997952	0.090492
200	1.799486	0.178760	1.964052	0.179930	1.981650	0.180046
500	3.853193	0.435440	4.761006	0.442614	4.868293	0.443332
1,000	6.040436	0.834169	9.057790	0.861940	9.471104	0.864767
2,000	7.774783	1.531658	16.409843	1.635555	17.944342	1.646498
5,000	7.230417	2.973732	30.567852	3.510122	38.346714	3.572143
10,000	5.023283	3.911947	37.216291	5.514902	59.804624	5.728592
20,000	2.640601	3.479769	27.519373	7.119665	75.972544	7.772893
50,000	1.115509	1.481306	4.926720	6.645443	67.006634	8.748347
100,000	0.990562	0.998241	0.865939	4.632321	41.527770	8.471943
200,000	1.000152	0.993609	0.955342	2.468199	16.017030	7.814921
500,000	1.000613	1.001117	1.011427	1.100285	1.743954	6.186772
1,000,000	1.000083	1.000274	1.002347	0.991426	0.905197	4.287471
2,000,000	0.999995	1.000021	1.000123	1.000202	1.008322	2.332665
5,000,000	0.999995	0.999995	0.999942	1.000547	1.005392	1.091438
10,000,000	0.999998	0.999998	0.999977	1.000073	1.000607	0.992274
20,000,000	1.000000	0.999999	0.999993	0.999995	0.999925	1.000177
50,000,000	1.000000	1.000000	0.999999	0.999996	0.999956	1.000492

and

$$(\phi c_t)=\frac{0.0002637\ k\ (t)_M}{\mu r_{sw}^2\ (t_D)_M}. \quad \ldots\ldots\ldots\ldots\ldots\ldots (42)$$

An estimate of the pseudospherical wellbore radius, r_{sw}, is also available if C and C_D are known.

$$r_{sw}=\left(\frac{0.44683C}{\phi c_t C_D}\right)^{1/3}. \quad \ldots\ldots\ldots\ldots\ldots\ldots (43)$$

C may be estimated from the type-curve match with the well-known unit-slope equation.

$$C=\frac{qB}{24}\left(\frac{t}{\Delta p}\right)_{\text{unit}}. \quad \ldots\ldots\ldots\ldots\ldots\ldots (44)$$

Note that standard field units have been used in Eqs. 41 through 44 and that B is the formation volume factor. With data from Table 9 and the match points indicated, a permeability of 91.5 md is computed from Eq. 41, which compares favorably with the true value of 88 md. From the time match (Eq. 42), the porosity/compressibility product is found, for the time match (in psi^{-1}),

$$\phi c_t=1.23\times10^{-6}.$$

With data from Table 9, for supplied data (in psi^{-1}),

$$\phi c_t=9.6\times10^{-7}.$$

With the fourth data point on Fig. 15 in Eq. 44, $C=0.106$ RB/psi is computed. As a check on the original value (in feet) of r_{sw}, Eq. 43 yields

$$r_{sw}=\left[\frac{(0.44683)(0.106)}{(9.6\times10^{-7})(1{,}000)}\right]^{1/3}=3.67.$$

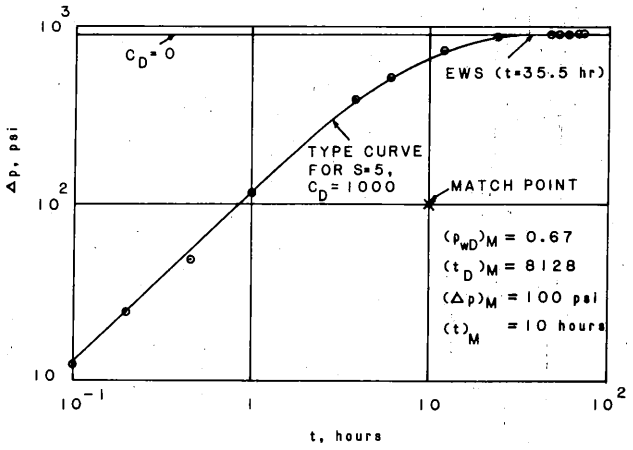

Fig. 15—Type curve match for pressure drawdown test (spherical flow).

This estimate of r_{sw} is in general agreement with the value shown in Table 9. Finally, the skin factor from the type-curve match ($s=5$) also agrees well with the true spherical skin factor of 4.8.

Because sufficient data are available for this test, the classic spherical flow analysis method[3,4,6,28] may be used. Therefore, the applicable drawdown equation in field units is

$$p_{wf}(t)=p_i-\frac{70.627\ qB\mu}{kr_{sw}}(1+s)+\frac{2{,}454.26\ qB\mu}{k}$$

$$\times\sqrt{\frac{\phi\mu c}{k}}\frac{1}{\sqrt{t}}. \quad \ldots\ldots\ldots\ldots\ldots\ldots (45)$$

TABLE 9—PRESSURE DRAWDOWN TEST (SPHERICAL FLOW)

t (hours)	p_{wf} (psia)	Δp (psi)
0.0	4,264.00	0.00
0.1	4,251.65	12.35
0.2	4,239.46	24.54
0.4	4,215.60	48.40
1.0	4,147.85	116.15
4.0	3,881.51	382.49
6.0	3,756.13	507.87
12.0	3,535.63	728.37
24.0	3,398.22	865.78
48.0	3,364.12	889.88
54.0	3,363.10	900.90
58.0	3,363.07	900.93
60.0	3,363.03	900.97
64.0	3,363.02	900.98
66.0	3,362.99	901.01
72.0	3,363.07	900.93

Well, fluid, and rock data	
q, STB/D	248
B, RB/STB	1.19
μ, cp	2.18
ϕ, fraction bulk volume	0.08
c_t, psi^{-1}	12×10^{-6}
r_{sw}, ft	3.327
r_w, ft	0.417
p_i, psia	4,264
h, ft	350
b, ft	28

Hence, a plot of p_{wf} vs. $1/\sqrt{t}$ on Cartesian paper should be linear, with slope m and intercept I given by

$$m=2{,}454.26\,\frac{qB\mu}{k^{3/2}}\sqrt{\phi\mu c} \quad \ldots\ldots\ldots\ldots\ldots\ldots (46)$$

and

$$I=p_i-\frac{70.627\,qB\mu}{kr_{sw}}(1+s). \quad \ldots\ldots\ldots\ldots\ldots\ldots (47)$$

Formation spherical permeability and damage skin factor can be computed from the slope and intercept, respectively.

$$k=\left(\frac{2{,}454.26\,qB\mu\sqrt{\phi\mu c}}{m}\right)^{2/3} \quad \ldots\ldots\ldots\ldots\ldots\ldots (48)$$

and

$$s=\left[\frac{(p_i-I)kr_{sw}}{70.627\,qB\mu}\right]-1. \quad \ldots\ldots\ldots\ldots\ldots\ldots (49)$$

The plot described above is shown in Fig. 16, from which $m=2.933$ psi(hr)$^{1/2}$ [20.2 kPa(hr)$^{1/2}$] and $I=3{,}362.67$ psi [23.2 MPa] were computed. With Eqs. 48 and 49, $k=84.65$ md and $s=4.59$ are calculated.

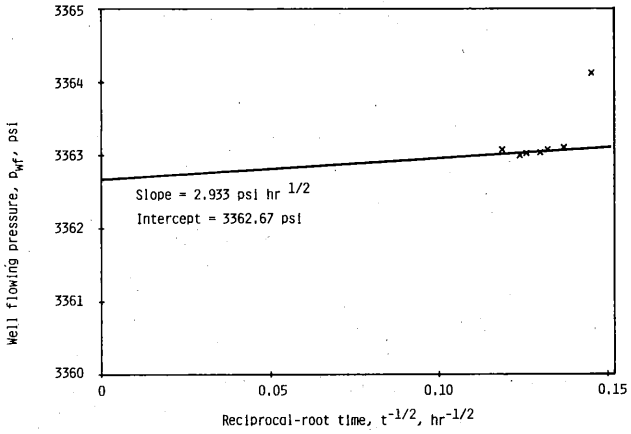

Fig. 16—Long-time spherical flow plot for pressure drawdown test.

These values are in excellent agreement with the true permeability and skin factor.

Observation

Our observation finds no parallel under cylindrical flow. Examination of a large number of data sets (for example, our Tables 1, 3, and 5 through 8 or Tables 16, 21, and 27 through 37 of Ref. 9) suggested the empirical relationship

$$p_{wD}(t_{Dw})\approx q_D(t_{Dw});\ s=0 \text{ and } t_D\gtrsim 1{,}000. \quad \ldots\ldots (50)$$

Eq. 50 states that the dimensionless wellbore pressure drop is approximately equal to the dimensionless sandface flow rate in undamaged spherical reservoirs inclusive of wellbore storage or phase redistribution effects. This relationship is sometimes valid for dimensionless time, t_D, as small as 500 but becomes more exact as t_D increases. Eq. 50 is empirical, and field verification is required.

Conclusions

Analytical expressions and type curves have been presented for the pressure and/or rate analysis of unsteady flow behavior in homogeneous and isotropic spherical reservoir systems. Skin effect, wellbore storage, and wellbore phase redistributions have been accounted for in the solutions. The most important equations are summarized here.

Eqs. 16, 20, and 37 can be used for well-pressure solutions with storage and skin, with long-time approximations, and with storage, skin, and phase redistribution, respectively. Eqs. 28 and 39 can be used for sandface flow rates with storage and skin and with storage, skin, and phase redistribution, respectively.

A new equation also was developed to estimate the duration of wellbore and near-wellbore effects under spherical flow exclusive of phase segregation. This investigation should be useful in the establishment of parity between spherical flow problems and its radial-cylindrical analog.

Although we have focused mainly on spherical flow, it should be noted that these methods extend to hemispherical flow with only minor modifications.

Hemispherical flow is identical to spherical flow with the obvious exception that the flow is contained within a hemisphere. Because the analysis is the same, the term "spherical flow" as used herein should be understood to encompass hemispherical flow as a special case. Finally, in undamaged spherical systems inclusive of wellbore storage and phase redistribution effects, dimensionless sandface flow rates and well pressures become identical after a t_D of about 1,000. This behavior appears unique to spherical flow.

Acknowledgment

Computer time required during this study was provided by the Petroleum Engineering Dept. at the U. of Missouri-Rolla.

Nomenclature

A = group defined by $1-e^{-2\sqrt{z}}$
b = group defined by the product pr; perforated interval, ft [m]
B = group defined by $1+e^{-2\sqrt{z}}$; formation volume factor
c, c_t = total system compressibility, atm^{-1} [Pa^{-1}]
C = coefficient of wellbore storage, cm^3/atm [res m^3/kPa]
C_{aD} = apparent dimensionless coefficient of wellbore storage
C_D = dimensionless coefficient of wellbore storage
C_ϕ = phase redistribution pressure parameter, atm [kPa]
$C_{\phi D}$ = dimensionless phase redistribution pressure parameter
C_1, C_2 = arbitrary constants, Eq. A-2
i = imaginary unit; $i=\sqrt{-1}$
I = intercept
k = undisturbed formation permeability, darcy
L = operator of the Laplace transformation
L^{-1} = operator of the inverse Laplace transformation
m = slope
n = index of summation
N = Stehfest algorithm parameter
p, p_{rt} = pressure, atm [kPa]
p_D = dimensionless formation pressure drop
$\bar{p}_D$ = Laplace transform of p_D
Δp_s = pressure drop across infinitesimal skin zone, atm [kPa]
p_{wD} = dimensionless wellbore pressure drop
$\bar{p}_{wD}$ = Laplace transform of p_{wD}
p_ϕ = phase redistribution pressure, atm [kPa]
$p_{\phi D}$ = dimensionless phase redistribution pressure
q = flow rate, cm^3/sec [stock-tank m^3/d]
q_a = annular rate of unloading, cm^3/sec [res m^3/d]
q_D = dimensionless sandface flow rate, Eq. 27
$\bar{q}_D$ = Laplace transform of q_D
q_{sf} = sandface flow rate, cm^3/sec [res m^3/d]
q_ϕ = phase redistribution flowrate, cm^3/sec [res m^3/d]
r = spherical spatial coordinate, in. [cm]
r_D = dimensionless spatial coordinate
r_{sw} = pseudospherical wellbore radius, in. [cm]
s = damage skin factor, dimensionless
t = time, sec
t_D = dimensionless time group
t_{Dw} = dimensionless time group, $(t_D)_{r=r_{sw}}$
T = spherical transmissivity group
$v(t)$ = arbitrary function, Eq. 18
$\bar{v}(z)$ = arbitrary transform, Eq. 18
z = variable of the Laplace transformation
α = constant, Eq. B-13
β = constant, Eq. 23
γ = phase redistribution time parameter, sec^{-1}
γ_D = dimensionless phase redistribution time parameter
Γ = gamma function
δ, γ = used in Eq. 18
Δ = difference
μ = viscosity, cp
ϕ = porosity, fraction bulk volume

Subscripts

a = annular
D = dimensionless
i = initial
M = match
sf = sandface
sw = pseudowellbore
wb = wellbore
ϕ = phase redistribution

References

1. Chatas, A.T.: "Unsteady Spherical Flow in Petroleum Reservoirs," *Soc. Pet. Eng. J.* (June 1966) 102-14; *Trans.*, AIME, **237**.
2. Moran, J.H. and Finklea, E.E.: "Theoretical Aspects of Pressure Phenomena Associated with the Wireline Formation Tester," *J. Pet. Tech.* (Aug. 1962) 899-908; *Trans.*, AIME, **225**.
3. Abbott, W.A., Collins, T., and Tippie, D.B.: "Practical Applications of Spherical Flow Transient Analysis," paper SPE 7485 presented at the 1978 SPE Annual Technical Conference and Exhibition, Houston, Oct. 1-3.
4. Culham, W.E.: "Pressure Buildup Equations for Spherical Flow Regime Problems," *Soc. Pet. Eng. J.* (Dec. 1974) 545-55.
5. Brigham, W.E. *et al.*: "The Analysis of Spherical Flow with Wellbore Storage," paper SPE 9294 presented at the 1980 SPE Annual Technical Conference and Exhibition, Dallas, Sept. 21-24.
6. Kohlhaas, C.A. and Abbott, W.A.: "Application of Linear and Spherical Flow Analysis Techniques to Field Problems," paper SPE 11088 presented at the 1982 SPE Annual Technical Conference and Exhibition, New Orleans, Sept. 26-29.
7. Goodrich, J.: "Time Intervals for Spherical Flow as a Function of Anisotropy and Well Completion Interval," paper SPE 11812 available from SPE, Richardson, TX, 1983.
8. Onyekonwu, M.O. and Horne, R.N.: "Pressure Response of a Reservoir with Spherically Discontinuous Properties," *J. Pet. Tech.* (Nov. 1983) 2127-34.
9. Joseph, J.A.: "Unsteady-State Cylindrical, Spherical and Linear Flow in Porous Media," PhD dissertation, U. of Missouri-Rolla (1984).

10. Meunier, D., Wittmann, M.J., and Stewart, G.: "Interpretation of Pressure Buildup Test Using In-Situ Measurement of Afterflow," *J. Pet. Tech.* (Jan. 1985) 143–52.
11. Stewart, G., Wittmann, M.J., and Meunier, D.: "Afterflow Measurement and Deconvolution in Well Test Analysis," paper SPE 12174 presented at the 1983 SPE Annual Technical Conference and Exhibition, San Francisco, Oct. 5–8.
12. Kucuk, F. and Ayestaran, L.: "Analysis of Simultaneously Measured Pressure and Sandface Flow Rate in Transient Well Testing," *J. Pet. Tech.* (Feb. 1985) 323–34.
13. Fetkovitch, M.J. and Vienot, M.E.: "Rate Normalization of Buildup Pressure Using Afterflow Data," *J. Pet. Tech.* (Dec. 1984) 2211–24.
14. Horne, R.N., Guillot, A., and Rosa, A.: "Computerized Well Test Analysis to Utilize Simultaneous Pressure and Flowrate Measurements," *Proc.*, 1983 New Zealand Geothermal Workshop, Auckland, N.Z. (Nov. 9–11).
15. Muskat, M.: *Physical Principles of Oil Production*, McGraw-Hill Book Co. Inc., New York City (1949).
16. Carslaw, H.S. and Jaeger, J.C.: *Conduction of Heat in Solids*, second edition, Oxford at the Clarendon Press, Oxford, England (1959).
17. Miller, F.G.: "Theory of Unsteady-State Influx of Water in Linear Reservoirs," *J. Inst. Pet.* (Nov. 1962) Vol. 48, No. 467, 365–79.
18. Rodriguez-N., R. and Carter, R.D.: "Unsteady Three-Dimensional Gas Flow in Thick Reservoirs," paper SPE 4266, available at SPE, Richardson, TX.
19. Joseph, J.A.: "Unsteady-State Cylindrical and Spherical Flow in Porous Media," Report No. USDI G1124129, Missouri Mining and Mineral Resources Research Inst., Rolla, MO, Oct. 1983.
20. Powers, D.L.: *Boundary Value Problems*, second edition, Academic Press, New York City (1979).
21. Carnahan, B., Luther, H.A., and Wilkes, J.O.: *Applied Numerical Methods*, John Wiley and Sons, New York City (1969).
22. Stehfest, Harald: "Algorithm 368—Numerical Inversion of Laplace Transforms [D5]," *Comm.*, Assoc. for Computing Machinery (Jan. 1970) **13**, No. 1, 47–49.
23. "Remark on Algorithm 368 [D5]—Numerical Inversion of Laplace Transforms," *Comm. Assoc. for Computing Machinery* (Oct. 1970) **13**, No. 10, 624.
24. Earlougher, R.C. Jr.: *Advances in Well Test Analysis*, SPE Monograph Series, SPE, Richardson (1977) **5**.
25. Hartree, D.R.: "Some Properties and Applications of the Repeated Integrals of the Error Function," *Memoirs and Proc., Manchester Lit. and Phil. Soc.* (1936) **80**, No. 9, 85–102.
26. Gautschi, Walter: "Algorithm 521: Repeated Integrals of the Coerror Function [S15]," Assoc. for Computing Machinery, *Trans. Math. Software* (Sept. 1977) **3**, No. 3, 301–02.
27. Carlile, R.E. and Gillett, B.E.: *Fortran and Computer Mathematics for the Engineer and Scientist*, Petroleum Publishing Co., Tulsa (1974).
28. Tippie, D.B., Collins, T., and Abbott, W.A.: "Pressure Transient Analysis in Bottom Water Drive Reservoir with Partial Completion," paper SPE 7487 presented at the 1978 SPE Annual Technical Conference and Exhibition, Houston, Oct. 1–3.
29. van Everdingen, A.F.: "The Skin Effect and Its Influence on the Productive Capacity of a Well," *J. Pet. Tech.* (June 1953) 171–76; *Trans.*, AIME, **198**.
30. Hurst, W.: "Establishment of the Skin Effect and Its Impedient to Fluid Flow into a Wellbore," *Petroleum Engineer* (Oct. 1953) B6–B16.
31. Ramey, H.J. Jr. and Agarwal, R.G.: "Annulus Unloading Rates as Influenced by Wellbore Storage and Skin Effect," *Soc. Pet. Eng. J.* (Oct. 1972) 453–62; *Trans.*, AIME, **253**.
32. Fair, W.B. Jr.: "Pressure Buildup Analysis With Wellbore Phase Redistribution," *Soc. Pet. Eng. J.* (Apr. 1981) 259–70.
33. Stegemeier, G.L. and Matthews, C.S.: "A Study of Anomalous Pressure Build-Up Behavior," *J. Pet. Tech.* (Feb. 1958) 44–50; *Trans.*, AIME, **213**.
34. Pitzer, S.C., Rice, J.D., and Thomas, C.E.: "A Comparison of Theoretical Pressure Build-Up Curves with Field Curves Obtained from Bottom-Hole Shut-In Tests," *J. Pet. Tech.* (Aug. 1959) 49–52; *Trans.*, AIME, **216**.
35. Thompson, L. *et al.*: "Analysis of Buildup Data Influenced by Wellbore Phase Redistribution," paper SPE 12782 presented at the 1984 SPE California Regional Meeting, Long Beach, April 11–13.
36. Abramowitz, M. and Stegun, I.A.: *Handbook of Mathematical Functions*, Dover Publ. Inc., New York City (1972).
37. Stewart, G. and Wittmann, M.: "Interpretation of the Pressure Response of the Repeat Formation Tester," paper SPE 8362 presented at the 1979 SPE Annual Technical Conference and Exhibition, Las Vegas, Sept. 23–26.

APPENDIX A

Laplace Transform Solution, Constant Surface Rate Case, Including Storage and Skin

Transform Eq. 5 over t_D and use the initial condition (Eq. 8).

$$\frac{d^2\bar{p}_D}{dr_D{}^2} - z\bar{p}_D = 0. \quad \text{(A-1)}$$

Eq. A-1 illustrates the fundamental operational property of the Laplace transformation, i.e., its reduction of a PDE to an ordinary one. Eq. A-1 is called a subsidiary equation; its general solution may be obtained by writing the indical equation for m. That is, because Eq. A-1 is linear and homogeneous with constant coefficients, assume a solution of the form $\bar{p}_D = e^{mr_D}$ or $m = \pm\sqrt{z}$. Therefore, the general solution to Eq. A-1 is

$$\bar{p}_D(r_D,z) = C_1 e^{-\sqrt{z}r_D} + C_2 e^{\sqrt{z}r_D}, \quad \text{(A-2)}$$

where C_1 and C_2 are arbitrary constants to be determined from the prescribed conditions, thereby providing the particular solution of interest. Transform the outer boundary condition Eq. 9.

$$\lim_{r_D \to 1} [\bar{p}_D(r_D,z)] = 0. \quad \text{(A-3)}$$

Substitute Eq. A-3 into Eq. A-2.

$$C_2 = -C_1 e^{-2\sqrt{z}}. \quad \text{(A-4)}$$

Substitute Eq. A-4 into the general solution (Eq. A-2).

$$\bar{p}_D(r_D,\ z) = C_1 \left[e^{-r_D\sqrt{z}} - e^{(r_D-2)\sqrt{z}} \right]. \quad \text{(A-5)}$$

Transform the auxiliary condition (Eq. 10).

$$\bar{p}_{wD}(z) = \bar{p}_D(r_D=0,\ z) - s\left[\frac{\partial \bar{p}_D}{\partial r_D}\right]_{r_D=0}. \quad \text{(A-6)}$$

Differentiate Eq. A-5 with respect to r_D, and evaluate at $r_D = 0$.

$$\left[\frac{d\bar{p}_D}{dr_D}\right]_{r_D=0} = -\sqrt{z}C_1\left(1+e^{-2\sqrt{z}}\right). \quad \text{(A-7)}$$

Substitute Eqs. A-5 and A-7 into Eq. A-6, and solve for the arbitrary constant, C_1.

$$C_1=\frac{\bar{p}_{wD}}{\left[1-e^{-2\sqrt{z}}+s\sqrt{z}\left(1+e^{-2\sqrt{z}}\right)\right]}. \quad \ldots\ldots (A\text{-}8)$$

Transform the inner boundary condition (Eq. 13).

$$zC_D\bar{p}_{wD}-\left[\frac{\partial\bar{p}_D}{\partial r_D}\right]_{r_D=0}=\frac{1}{z}. \quad \ldots\ldots\ldots\ldots (A\text{-}9)$$

Substitute Eq. A-8 into Eq. A-7 and the resulting expression into Eq. A-9 to obtain the solution for the well flowing-pressure transform $\bar{p}_{wD}$.

$$\bar{p}_{wD}(z)=\frac{\left(1-e^{-2\sqrt{z}}\right)+s\sqrt{z}\left(1+e^{-2\sqrt{z}}\right)}{z^{3/2}\left\{\sqrt{z}C_D\left[\left(1-e^{-2\sqrt{z}}\right)+s\sqrt{z}\left(1+e^{-2\sqrt{z}}\right)\right]+\left(1+e^{-2\sqrt{z}}\right)\right\}}. \quad \ldots\ldots\ldots\ldots\ldots\ldots\ldots (A\text{-}10)$$

We may simplify Eq. A-10 by setting $A=1-e^{-2\sqrt{z}}$ and $B=1+e^{-2\sqrt{z}}$ so that

$$\bar{p}_{wD}(z)=\frac{A+s\sqrt{z}B}{z^{3/2}\left[\sqrt{z}C_D\left(A+s\sqrt{z}B\right)+B\right]}. \quad \ldots\ldots (A\text{-}11)$$

This result is presented in the text as Eq. 16. Eq. A-11 is valid for $C_D\geqq 0$ and $s\geqq 0$. We may also determine the transform of the formation pressure drop—i.e., $\bar{p}_D(r_D\geqq 0^+,\ z)$—by eliminating $\bar{p}_{wD}$ instead of $\bar{p}_D(r_D=0,\ z)$ above. When this is done, the arbitrary constant C_1 becomes

$$C_1=\frac{1}{z^{3/2}\left[\sqrt{z}C_D\left(A+s\sqrt{z}B\right)+B\right]}. \quad \ldots\ldots (A\text{-}12)$$

Substitute Eq. A-12 into the general solution (Eq. A-5).

$$\bar{p}_D(r_D,z)=\frac{e^{-r_D\sqrt{z}}-e^{(r_D-2)\sqrt{z}}}{z^{3/2}\left[\sqrt{z}C_D\left(A+s\sqrt{z}B\right)+B\right]};$$

$$r_D\geqq 0^+. \quad \ldots\ldots\ldots\ldots\ldots\ldots\ldots (A\text{-}13)$$

This result is presented in the text as Eq. 17. Eq. A-13 is valid for $C_D\geqq 0$, $s\geqq 0$, and $0^+\leqq r_D\leqq 1$. The notation 0^+ should be interpreted as those values of r_D that fall on the formation side of the infinitesimal skin zone. Eq. A-13 reduces to Eq. A-11 when $s=0$ and $r_D=0$, for $C_D\geqq 0$.

APPENDIX B

Asymptotic Behavior of Eq. 16

Our purpose here is to derive short- and long-time approximation equations for spherical flow with storage and skin (Eq. 16). For convenience, Eq. 16 is rewritten to the following form.

$$\bar{p}_{wD}(z)=\text{Term I}+\text{Term II}, \quad \ldots\ldots\ldots\ldots\ldots (B\text{-}1)$$

where

$$\text{Term I}=\frac{1-e^{-2\sqrt{z}}}{\text{DENOM}} \quad \ldots\ldots\ldots\ldots\ldots\ldots (B\text{-}2)$$

and

$$\text{Term II}=\frac{s\sqrt{z}(1+e^{-2\sqrt{z}})}{\text{DENOM}}, \quad \ldots\ldots\ldots\ldots (B\text{-}3)$$

with

$$\text{DENOM}=z^2C_D(1-e^{-2\sqrt{z}})+sC_Dz^{5/2}\times(1+e^{-2\sqrt{z}})+z^{3/2}(1+e^{-2\sqrt{z}}). \quad \ldots\ldots\ldots\ldots (B\text{-}4)$$

Particular approximation forms are produced by investigating Eq. B-1 as $z\to\infty$ (short time) and as $z\to 0$ (long time), and constructing the real-time solution from the linearity property of the inverse Laplace transformation.

$$p_{wD}(t_D)=L^{-1}(\text{Term I})+L^{-1}(\text{Term II}). \quad \ldots\ldots (B\text{-}5)$$

Short-Time Approximation ($z\to\infty$). As $z\to\infty$, the denominator (Eq. B-4) can be approximated by the term involving the largest power of z. Hence,

$$\text{DENOM}\to z^2C_D;\ s=0 \quad \ldots\ldots\ldots\ldots\ldots\ldots (B\text{-}6)$$

and

$$\text{DENOM}\to sC_Dz^{5/2};\ s>0, \quad \ldots\ldots\ldots\ldots\ldots (B\text{-}7)$$

because the negative exponential decays rapidly as its argument increases—i.e., terms $0(e^{-2\sqrt{z}})$ safely can be neglected. Term I (Eq. B-2), therefore, can be written as

$$\text{Term I}=\frac{1}{z^2C_D};\ s=0 \quad \ldots\ldots\ldots\ldots\ldots\ldots (B\text{-}8)$$

and

$$\text{Term I}=\frac{1}{sC_Dz^{5/2}};\ s>0. \quad \ldots\ldots\ldots\ldots\ldots (B\text{-}9)$$

The inverse Laplace transform of Eq. B-8 can be written directly as

$$L^{-1}(\text{Term I})=\frac{t_D}{C_D};\ s=0. \quad \ldots\ldots\ldots\ldots\ldots (B\text{-}10)$$

The inverse transform for the second form of Term I when $s>0$ (Eq. B-9) is available from tables in Ref. 36.

$$L^{-1}\left(\frac{1}{sC_D z^{5/2}}\right)=\frac{1}{sC_D}(4t_D)^{3/2}\mathrm{i}^3\mathrm{erfc}(0), \quad \ldots(\text{B-11})$$

where $\mathrm{i}^3\mathrm{erfc}$ is an iterated coerror function.[25,26,36] However,

$$\mathrm{i}^3\mathrm{erfc}(0)=\frac{1}{2^3\Gamma(5/2)}, \quad \ldots\ldots\ldots\ldots\ldots\ldots(\text{B-12})$$

where Γ denotes the gamma function.[36] Because $\Gamma(5/2)=3\sqrt{\pi}/4$, Eq. B-12 becomes

$$\mathrm{i}^3\mathrm{erfc}(0)=\frac{1}{6\sqrt{\pi}}. \quad \ldots\ldots\ldots\ldots\ldots\ldots\ldots(\text{B-13})$$

Substitute Eq. B-13 into Eq. B-11 to obtain

$$L^{-1}(\text{Term I})=\frac{4}{3\sqrt{\pi}sC_D}t_D{}^{3/2}; \quad s>0. \quad \ldots\ldots(\text{B-14})$$

To obtain the complete solution, Term II must be constructed next. If $s=0$,

$$\text{Term II}=0; \quad s=0, \quad \ldots\ldots\ldots\ldots\ldots\ldots(\text{B-15})$$

whose inverse is also identically zero. For $s>0$, Term II can be written from Eqs. B-3 and B-7.

$$\text{Term II}=\frac{s\sqrt{z}(1+e^{-2\sqrt{z}})}{sC_D z^{5/2}},$$

which can be simplified further to yield

$$\text{Term II}=\frac{1}{z^2 C_D}; \quad s>0. \quad \ldots\ldots\ldots\ldots\ldots\ldots(\text{B-16})$$

The inverse transform of Eq. B-16 is

$$L^{-1}(\text{Term II})=\frac{t_D}{C_D}; \quad s>0. \quad \ldots\ldots\ldots\ldots\ldots(\text{B-17})$$

The complete short-time approximation is constructed in accordance with Eq. B-5.

$$p_{wD}(t_D)=\frac{t_D}{C_D}; \quad s=0 \quad \ldots\ldots\ldots\ldots\ldots\ldots(\text{B-18})$$

and

$$p_{wD}(t_D)=\frac{t_D}{C_D}+\frac{4}{3\sqrt{\pi}sC_D}t_D{}^{3/2}; \quad s>0. \quad \ldots\ldots(\text{B-19})$$

Although Eq. B-19 can be a useful approximating form, it is evident that Eqs. B-18 and B-19 can be combined to provide a general, early-time equation, provided that terms $0(t_D{}^{3/2})$ can be neglected. Hence,

$$p_{wD}(t_D)=\frac{t_D}{C_D}; \quad s\geqq 0 \text{ and } C_D\neq 0. \quad \ldots\ldots\ldots(\text{B-20})$$

This result is presented as Eq. 19 in the main text.*

Long-Time Approximation ($z\to 0$). As $z\to 0$, the denominator (Eq. B-4) can be approximated by the term involving the smallest power of z. Hence,

$$\text{DENOM}\to 2z^{3/2}. \quad \ldots\ldots\ldots\ldots\ldots\ldots\ldots(\text{B-21})$$

Term I (Eq. B-2), therefore, can be written as

$$\text{Term I}=\frac{1}{2z^{3/2}}-\frac{e^{-2\sqrt{z}}}{2z^{3/2}}. \quad \ldots\ldots\ldots\ldots\ldots(\text{B-22})$$

The inverse Laplace transform of Eq. B-22 is[36]

$$L^{-1}\left(\frac{1}{2z^{3/2}}\right)=\sqrt{\frac{t_D}{\pi}} \quad \ldots\ldots\ldots\ldots\ldots\ldots(\text{B-23})$$

$$L^{-1}\left(\frac{e^{-2\sqrt{z}}}{2z^{3/2}}\right)=\sqrt{\frac{t_D}{\pi}}e^{-1/t_D}-\mathrm{erfc}\left(\frac{1}{\sqrt{t_D}}\right). \quad \ldots\ldots\ldots\ldots\ldots\ldots\ldots\ldots(\text{B-24})$$

Erfc is given by

$$\mathrm{erfc}(y)=\frac{2}{\sqrt{\pi}}\int_y^\infty e^{-\beta^2}\,d\beta. \quad \ldots\ldots\ldots\ldots(\text{B-25})$$

The inverse Laplace transform of Eq. B-22 is, therefore,

$$L^{-1}(\text{Term I})=\sqrt{\frac{t_D}{\pi}}(1-e^{-1/t_D})\mathrm{erfc}\left(\frac{1}{\sqrt{t_D}}\right). \quad \ldots\ldots\ldots\ldots\ldots\ldots\ldots\ldots(\text{B-26})$$

Term II is written directly from Eqs. B-3 and B-21.

$$\text{Term II}=\frac{s\sqrt{z}(1+e^{-2\sqrt{z}})}{2z^{3/2}},$$

which can be simplified to produce

$$\text{Term II}=\frac{s}{z}. \quad \ldots\ldots\ldots\ldots\ldots\ldots\ldots(\text{B-27})$$

*An identical result was obtained in the earlier version of this paper (SPE 12950) by allowing $s\to\infty$.

The inverse transform of Eq. B-27 is

$$L^{-1}(\text{Term II})=s. \quad \ldots\ldots\ldots\ldots\ldots\ldots\ldots\ldots (B\text{-}28)$$

The complete long-time approximation is constructed from Eq. B-5.

$$p_{wD}(t_D)=\sqrt{\frac{t_D}{\pi}}(1-e^{-1/t_D})+\text{erfc}\left(\frac{1}{\sqrt{t_D}}\right)+s. \quad \ldots\ldots\ldots\ldots\ldots\ldots\ldots\ldots (B\text{-}29)$$

This result is presented in the main text as Eq. 20.*

The customary forms, $s=0$, of the classic spherical source solution[2,8,16,37] are all available from Eq. B-29 as special cases. For example, at large t_D (small $1/t_D$), the exponential in the first term of Eq. B-29 can be written as $[1-(1/t_D)]$, and the first term in Eq. B-29 becomes

$$\sqrt{\frac{t_D}{\pi}}(1-e^{-1/t_D})=\frac{1}{\sqrt{\pi t_D}}. \quad \ldots\ldots\ldots\ldots\ldots\ldots (B\text{-}30)$$

Similarly, at large t_D, the complementary error function can be written as[16]

$$\text{erfc}\left(\frac{1}{\sqrt{t_D}}\right)=1-\frac{2}{\sqrt{\pi t_D}}. \quad \ldots\ldots\ldots\ldots\ldots (B\text{-}31)$$

Using Eqs. B-30 and B-31 in Eq. B-29, with $s=0$, we obtain

$$p_{wD}(t_D)=1-\frac{1}{\sqrt{\pi t_D}}, \quad \ldots\ldots\ldots\ldots\ldots\ldots (B\text{-}32)$$

which is the classic long-time approximation for spherical or point sources.[37] Using Eq. B-29, which was derived for long time, as a starting point, we can also derive the classic ($s=0$) short-time spherical source solution[8].

$$\sqrt{\frac{t_D}{\pi}}(1-e^{-1/t_D})=\sqrt{\frac{t_D}{\pi}} \quad \ldots\ldots\ldots\ldots\ldots\ldots (B\text{-}33)$$

and

$$\text{erfc}\left(\frac{1}{\sqrt{t_D}}\right)=\sqrt{\frac{t_D}{\pi}} \quad \ldots\ldots\ldots\ldots\ldots\ldots (B\text{-}34)$$

Using Eqs. B-33 and B-34 in Eq. B-29 with $s=0$, we have

$$p_{wD}(t_D)=2\sqrt{\frac{t_D}{\pi}}, \quad \ldots\ldots\ldots\ldots\ldots\ldots (B\text{-}35)$$

*A rigorous approximation equation involving an infinite sum of iterated coerror functions was presented in the earlier version of this paper (SPE 12950) by allowing $C_D=0$. Eq. B-29 derived in this Appendix is more tractable and, hence, is preferable.

which is the desired result. Finally, at infinite time, Eq. B-29 becomes

$$\lim_{t_D\to\infty}[p_{wD}(t_D)]=1+s. \quad \ldots\ldots\ldots\ldots\ldots\ldots (B\text{-}36)$$

This result is discussed further in the main text.

APPENDIX C
The Dimensionless Sandface Flow Rate

We discussed earlier the wellbore mass conservation yielding the equation

$$\frac{q_a}{q}+\frac{q_{sf}}{q}=1, \quad \ldots\ldots\ldots\ldots\ldots\ldots\ldots (C\text{-}1)$$

where unity represents the constant dimensionless surface flow rate (i.e., q/q). Eq. C-1 is the inner boundary (Neumann) condition, and when expressed in terms of the dimensionless variables defined before, Eq. 13 results in

$$C_D\frac{dp_{wD}}{dt_D}-\left(\frac{\partial p_D}{\partial r_D}\right)_{r_D=0}=1.$$

Therefore, we may write the dimensionless sandface flow rate explicitly in two equivalent forms:

$$q_D(t_D)=-\left(\frac{\partial p_D}{\partial r_D}\right)_{r_D=0}$$

and

$$q_D(t_D)=1-C_D\frac{dp_{wD}}{dt_D}, \quad \ldots\ldots\ldots\ldots\ldots\ldots (C\text{-}2)$$

where

$$q_D(t_D)=\frac{q_{sf}(t_D)}{q}. \quad \ldots\ldots\ldots\ldots\ldots\ldots\ldots (C\text{-}3)$$

Transform Eqs. 11 and C-2 over t_D, and let $\bar{q}_D(z)$ be the Laplace transformation of $q_D(t_D)$.

$$\bar{q}_D(z)=-\left(\frac{\partial \bar{p}_D}{\partial r_D}\right)_{r_D=0}. \quad \ldots\ldots\ldots\ldots\ldots\ldots (C\text{-}4)$$

$$\bar{q}_D(z)=\frac{1}{z}-zC_D\bar{p}_{wD}(z). \quad \ldots\ldots\ldots\ldots\ldots\ldots (C\text{-}5)$$

In Appendix A, expressions were derived both for $\bar{p}_D(r_D, z)$ and for $\bar{p}_{wD}(z)$. The explicit forms for $\bar{q}_D$, therefore, are available when Eq. A-13 is differentiated

once with respect to r_D, evaluated at $r_D=0$, and introduced into Eq. C-4 and when Eq. A-11 is substituted directly into Eq. C-5.

$$\bar{q}_D(z)=\frac{B}{z\left[\sqrt{z}C_D(A+s\sqrt{z}B)+B\right]}. \quad \ldots\ldots\ldots (C\text{-}6)$$

$$\bar{q}_D(z)=\frac{1}{z}-\frac{C_D(A+s\sqrt{z}B)}{\left[zC_D(A+s\sqrt{z}B)+\sqrt{z}B\right]}, \quad \ldots\ldots\ldots (C\text{-}7)$$

with $A=1-e^{-2\sqrt{z}}$ and $B=1+e^{-2\sqrt{z}}$ as before. Observe from Eqs. C-6 and C-7 that for $C_D=0$, $\bar{q}_D(z)=1/z$, so $q_D(t_D)=1$, implying that the sandface and surface rates are identical ($q_{sf}=q$). Eqs. C-6 and C-7 are valid for $s\geq 0$ and $C_D\geq 0$, at $r_D=0$.

APPENDIX D

Laplace Transform Solution, Phase Redistribution

The procedure of Appendix A is followed until Eq. A-8. Now differentiate Eq. 34 with respect to t_D and substitute the result into Eq. 36.

$$C_D\frac{dp_{wD}}{dt_D}-\left(\frac{\partial p_D}{\partial r_D}\right)_{r_D=0}-\gamma_D C_D C_{\phi D}e^{-\gamma_D t_D}=1. \quad \ldots\ldots\ldots (D\text{-}1)$$

Transform the new redistribution inner boundary condition (Eq. D-1).

$$zC_D\bar{p}_{wD}-\left(\frac{\partial \bar{p}_D}{\partial r_D}\right)_{r_D=0}-\frac{\gamma_D C_D C_{\phi D}}{z+\gamma_D}=\frac{1}{z}; \quad z>-\gamma_D. \quad \ldots\ldots\ldots (D\text{-}2)$$

Next, substitute Eq. A-8 into Eq. A-7 and then the resulting expression into Eq. D-2 to obtain the solution for the transform of the well flowing-pressure drop.

$$\bar{p}_{wD}(z)=\frac{(\gamma_D C_{aD}+zC_D)(A+s\sqrt{z}B)}{(zC_{aD})(z+\gamma_D)[zC_D(A+s\sqrt{z}B)+\sqrt{z}B]}; \quad C_{aD}\neq 0, \quad \ldots\ldots\ldots (D\text{-}3)$$

where A and B are as defined in Appendix A and in the main text, and C_{aD} is as defined in Eq. 40. The solution for the formation pressure drop is derived in Ref. 9 and is presented in the text as Eq. 38. Eq. 36 can be solved for the dimensionless sandface flow rate as

$$-\left(\frac{\partial p_D}{\partial r_D}\right)_{r_D=0}=\frac{q_{sf}}{q}=q_D(t_D)$$

$$=1-C_D\left(\frac{dp_{wD}}{dt_D}-\frac{dp_{\phi D}}{dt_D}\right). \quad \ldots\ldots\ldots (D\text{-}4)$$

The transform of $q_D(t_D)$ is obtained by differentiating the negative of Eq. 38 with respect to r_D, and evaluating the result at $r_D=0$.

$$\bar{q}_D(z)=\frac{(\gamma_D C_{aD}+zC_D)B}{(zC_{aD})(z+\gamma_D)[\sqrt{z}C_D(A+s\sqrt{z}B)+B]}; \quad C_{aD}\neq 0. \quad \ldots\ldots\ldots (D\text{-}5)$$

Eqs. D-3 and D-5 are presented as Eqs. 37 and 39, respectively, in the text. Further details of these derivations are available in Ref. 9.

SI Metric Conversion Factors

ft	×	3.048*	E−01	= m
psi	×	6.894 757	E+00	= kPa
psi^{-1}	×	1.450 377	E−04	= Pa^{-1}
STB	×	1.589 873	E−01	= m^3

*Conversion factor is exact.

SPEJ

Original manuscript (SPE 12950) received in the Society of Petroleum Engineers office Feb. 28, 1984. Paper accepted for publication Jan. 9, 1985. Revised manuscript received Nov. 20, 1984.